J. Fluid Mech. (1999), *vol.* 384, *pp.* 27–58. Printed in the United Kingdom

The focusing of surface waves by internal waves

By A. N. DONATO, D. H. PEREGRINE† AND J. R. STOCKER

School of Mathematics, University of Bristol, University Walk, Bristol BS8 1TW, UK

(Received 28 January 1998 and in revised form 15 October 1998)

The surface current generated by internal waves in the ocean affects surface gravity waves. The propagation of short surface waves is studied using both simple ray theory for linear waves and a fully nonlinear numerical potential solver. Attention is directed to the case of short waves with initially uniform wavenumber, as may be generated by a strong gust of wind. In general, some of the waves are focused by the surface current and in these regions the waves steepen and may break. Comparisons are made between ray theory and the more accurate solutions. For ray theory, the occurrence of focusing is examined in some detail and exact analytic solutions are found for rays on currents with linear and quadratic spatial variation – only the latter giving focusing for our initial conditions. With regard to interpretation of remote sensing of the sea surface, we find that enhanced wave steepness is not necessarily associated with a particular phase of the internal wave, and simplistic interpretations may sometimes be misleading.

1. Introduction

Internal waves propagate on density gradients beneath the sea surface. The waves may be caused by ships in the case of shallow pycnoclines in estuarine regions, or perhaps by tidal flow over the edge of the continental shelf disturbing a deeper (~ 100 m) thermocline in a warm ocean. A strong gust of wind over the sea surface may generate a set of short waves of initially approximately uniform wavenumber. We are concerned with the propagation of short waves over an internal wave. Our aim is towards a better understanding of the resultant sea surface in order to compare with radar images of the water surface over internal waves.

Figure 1 shows a photograph taken from an aeroplane flying at an altitude of approximately 8 km off the coast of Maine, USA. It shows the focusing effect underlying internal waves have on the sea surface. In this case, the internal waves were probably generated by tidal flow over the edge of the continental shelf. The internal waves and hence surface current, have a wavelength of some kilometres. It is possible to see the effect of the internal wave due to the sun glitter on the sea surface which has become rougher in regions of focusing. Internal waves are also often observed due to surface oil slicks: the surface current caused by the internal wave concentrates the oil and other surface debris in regions of convergence. The numerous field observations include those by Osborne & Burch (1980) who recorded internal solitary waves in the Andaman sea. More recent studies include those by Watson & Robinson (1990) and Watson (1994). Field data from the internal waves

† Author to whom correspondence should be addressed, e-mail: d.h.peregrine@bris.ac.uk.

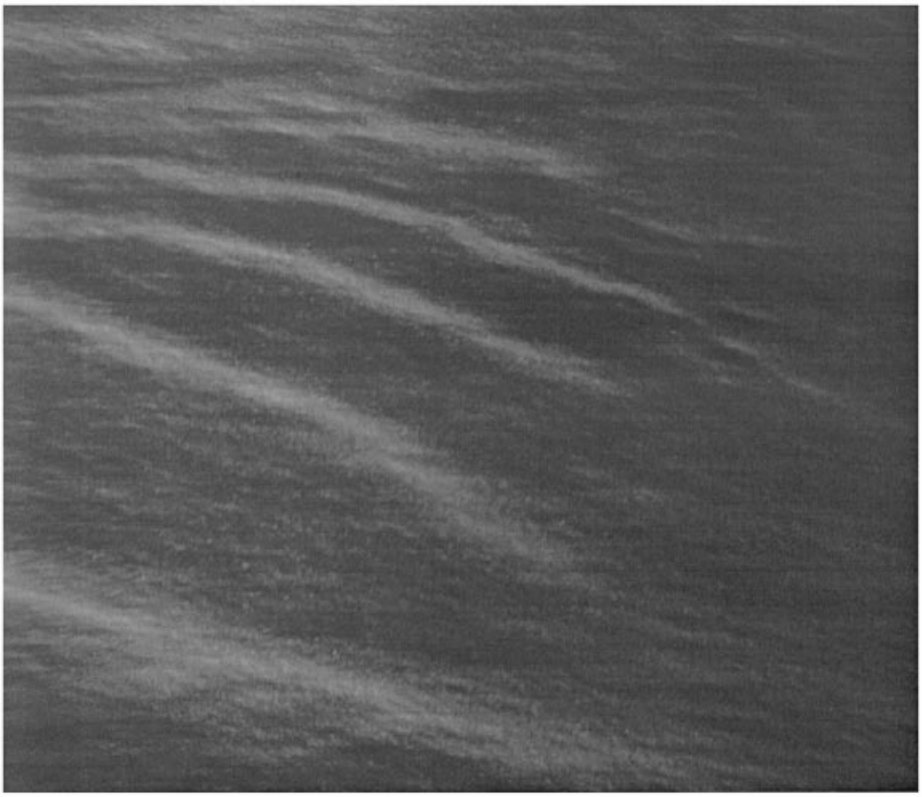

FIGURE 1. Aerial photograph taken off the coast of Maine, USA, showing the effect of underlying internal waves on the sea surface (D.H.P., 30 September 1996).

propagating through the Strait of Gibraltar were obtained using radar and sound imaging. Good agreement was found between theoretical and experimental predictions of phase speed. Internal wave wakes were generated by three ships in Loch Linnhe, Scotland in order to take SAR images of the surface and results were analysed using theory and *in situ* internal wave measurements in Watson, Chapman & Apel (1992) and Hogan *et al.* (1996).

Much work has also been done on the radar manifestations of internal waves, for example Alpers (1985) proposed a theory of radar imaging based on a simple compression and stretching model for the effect of an internal wave on the surface waves. Other modelling work includes the use of data from the SAR internal wave signature experiment (SARSEX) in the New York Bight (for further references see an overview of the experiment by Gasparovic, Apel & Kasischke 1988) and data from SAR images of internal waves in Georgia Strait, British Columbia (see, for example, Shuchman *et al.*, 1988).

Another effect that is apparent on the sea surface is ripple damping due to the presence of an organic film. We do not include such effects.

The interaction of water waves and currents is the subject of two substantial reviews. Peregrine (1976) is a very wide ranging review discussing a range of topics. Jonsson (1990) gives a more focused account in the context of ocean and coastal problems. The first complete set of equations to describe short waves propagating over much larger scale, non-uniform currents were given by Longuet-Higgins & Stewart,

summarized in their 1964 paper. It is found that wave energy is not conserved, so they introduced the concept of 'radiation stress' to describe the momentum flux (or Reynolds stress) terms which give the exchange of momentum with the current. Later, the concept of wave action was developed by Bretherton & Garrett (1968) who show that it is conserved for non-dissipative waves travelling over slowly varying currents. Many of the theoretical approaches include this energy transfer between the surface waves and the internal waves, e.g. Rizk & Ko (1978). This coupling can cause a change in form of the internal wave. In this work we do not consider the effect of this energy transfer on the internal waves, and the surface waves are modified by the internal wave which is treated as a given surface current. The fluid is taken to be inviscid.

Although the modelling described in this paper only makes use of the surface current, we put our computations in context by considering the internal waves to be propagating on the interface between two layers of differing constant density. This two-layer model assumes that the upper layer is fully mixed, which is usually appropriate because of the mixing effects of surface wave breaking. It is straightforward to obtain the velocity potential in the upper and lower layers as the flow is assumed to be irrotational since it is only the near-surface velocity field which is relevant for short surface waves. The surface current is unidirectional, with a sinusoidal spatial variation which moves at the internal wave phase velocity.

Gargett & Hughes (1972) used the same two-layer model for the internal wave as we choose here. They considered a constant-frequency initial condition for the surface waves, whereas we consider a constant-wavenumber initial condition which gives a more generic form of solution and leads to focusing of the surface waves.

A recent paper by White & Fornberg (1998) discusses some interesting results related to those presented here. They consider the interaction between surface gravity waves and a region of two-dimensional unsteady surface current with random fluctuations from a small (sometimes zero) mean. Their method involves statistical analysis of the distance to focus which is analogous to the time to focus that we consider in the present work. They show that the probability distribution for the formation of a freak wave – formed from the concentration of wave action in a caustic region – does not depend on the statistics of the current.

Two approaches to modelling surface waves, for the two-dimensional case, are described. First, we use a fully nonlinear potential solver to model the surface waves in the system. Although computationally intensive, this method gives accurate results which include nonlinear effects such as the early stages of breaking, which is relevant to specular radar scattering – 'twinkling'. The computations stop as the waves break, when the surface curvature becomes too high to resolve numerically. Secondly, we obtain solutions using linear ray theory, which is the simplest approach to the investigation of the time and position of the focusing of the waves. The disadvantage of this theory is that it is linear and, in addition, solutions are not valid at a focus or on caustics where the ray approximation becomes singular and uniform approximations are required to obtain full solutions to the linear equations. In practice such uniform approximations may be found, but since we have the accurate nonlinear solutions they are not derived here.

We investigate the effects on the surface waves of varying the strength and wavelength of the internal wave. The initial steepness and wavelength of the short waves are also studied. By choosing this particularly simple initial state, we reduce the problem to one with three dimensionless parameters: two velocity ratio parameters and

the initial steepness of the short waves. Details of the problem and the approaches we use are given in § 2.

In § 3 we give a typical example and use this example as a reference for discussion of variations in the wave and current parameters. The effects of nonlinearity, steepness and wave breaking are discussed in § 4. In § 5, we obtain exact solutions of linear ray theory for currents with linear and quadratic spatial variation. Results for reflection of rays are given in terms of a velocity-ratio parameter space diagram. Ray-theory predictions for the time and position of focusing and general trends in terms of varying the two velocity-ratio parameters are given in § 6. Conclusions are given in § 7.

2. Governing equations

2.1. *The two-layer model of the internal wave*

Consider a two-layer model of a stratified ocean. For modelling two-dimensional motion, an $(\hat{x}, y)$ coordinate system is chosen with $\hat{x}$ measured horizontally along the undisturbed free surface and y measured vertically upwards. The frequency, wavelength and wavenumber of a sinusoidal internal wave are taken to be Ω, Λ and K respectively where $K = 2\pi/\Lambda$. The phase speed of the internal wave $V = \Omega/K$ is normally very much less than that of surface waves of the same wavenumber. The interface between the two fluids is perturbed slightly so that the problem may be linearized, and a normal mode representation is taken for the velocity potentials in the upper and lower layers (depths h_1 and h_2 respectively), and the elevation $y = Y(\hat{x}, t)$ of the interface. Application of Laplace's equation, the linearized dynamic and kinematic boundary conditions, gives the dispersion relation which can be solved in the limit $h_2 \to \infty$ to obtain Ω^2:

$$\Omega^2 = \frac{gK(\rho_2 - \rho_1)}{\rho_1 + \rho_2 \coth K h_1}, \tag{1}$$

where ρ_1 and ρ_2 are the densities in the upper and lower layers respectively. We obtain well-known, analytic forms for the surface elevation $\eta(\hat{x}, t)$ and the velocity potential ϕ_1 in the upper layer, which are used throughout the paper. This leads to a surface current of the form

$$\left.\frac{\partial \phi_1}{\partial \hat{x}}\right|_{y=h_1} = U_c \cos(K\hat{x} - \Omega t). \tag{2}$$

For much of the analysis and presentation of results, we choose a frame of reference (x, t) moving with the phase speed, V, of the surface current, where $x = \hat{x} - Vt$. In this frame of reference, the current becomes steady: $U(x) = U_c \cos(Kx) - V$ and we are able to draw the streamlines in the flow (see figure 3). A steady current is also useful when looking for analytical results using linear ray theory. Where applicable, at least one period of the internal wave is shown and often two wavelengths are included.

We take the wavelength, λ, of the short gravity waves to be much less than the depth, h_1, of the upper layer. Thus the waves themselves have no effect on the stratification at $y = h_1$. However, the higher-order modulation induced by a non-uniform wave train is on a larger scale and may, in time, change the form of the internal wave. It is possible to add in a linear perturbation due to this modulation and thus model the change in wave form of the internal wave. However, for this unsteady problem of an initially constant-wavenumber wave train, we do not expect to see any large effects due to this modulation, even in the resonant case, so we have not included the

relevant terms in this work. Note also that this velocity potential is also applicable to modelling a gradually stratified ocean as the internal waves are sinusoidal, and there is a sufficiently deep upper layer of constant density.

2.2. *Nonlinear calculations*

In order to model surface waves on a current due to an internal wave, an accurate numerical method which computes the evolution of steep, unsteady waves on irrotational flow was extended to include the potential, ϕ_1, for the internal wave. The original non-linear code solves Laplace's equation in a spatially periodic domain (see Dold & Peregrine 1986 and Dold 1992). Fully nonlinear boundary conditions are applied at the free surface and a uniform condition (e.g. a fixed bed or zero velocity at great depth) is applied at the lower boundary. The solution method is based on solving an integral equation that arises from Cauchy's integral theorem for functions of a complex variable. Full details are in Dold (1992) including a discussion of the stability of the scheme for long-duration computations such as are presented here.

In order to apply Cauchy's integral theorem to the problem in a bounded domain, the potential, ϕ, must be known on all the boundaries. The kinematic and Bernoulli boundary conditions are applied at the surface, and the periodic domain condition leads to the cancellation of any contribution to the integral at the vertical boundaries. When no internal wave is present, the potential on the lower boundary can either be found by reflection, in the case of finite depth, or by applying the condition $\phi \to 0$ for very deep water. Here we are considering short waves with a wavelength much less than the upper layer depth so we suppose that for large depth $\phi \to \phi_1$. This is non-physical for points in the lower layer and means that we are neglecting interactions which modify the internal waves as discussed above.

Initially, for each time step, the 'total' potential $\phi = \phi_w + \phi_1$ is known on the surface. The internal wave potential, ϕ_1, is then subtracted from the surface value of ϕ to leave ϕ_w, the remaining surface wave potential which satisfies $\phi_w \to 0$ as $y \to -\infty$. Laplace's equation is satisfied by ϕ_w so Cauchy's integral theorem may be used to obtain $\nabla\phi_w$ on the free surface. The potential due to the internal wave is then added back in and corresponding 'total' velocities are evaluated. The kinematic and dynamic boundary conditions on the surface can then be used to time step the 'total' potential. Once an accurate, converged solution has been obtained for the 'total' potential on the surface, the cycle can begin again.

The free surface is discretized with computational points which are labelled in terms of a Lagrangian parameter. This means the surface discretization points tend to drift with the current. If there is no underlying current, the drift will be on a local scale relative to the surface waves, but with the large-scale currents, owing to the internal waves, the points converge and diverge with the surface current. Figure 3 shows the streamlines of the underlying current which influences the drift of the surface points. This soon gives bad resolution of the surface waves, so the program has been developed to incorporate a redistribution of points along the surface at regular intervals in time using a tenth-order interpolation algorithm to preserve full accuracy. In order to maintain accuracy over long integration times, fine discretization and a small tolerance parameter are used. No smoothing is used.

Initial conditions for the computations are an initial shape for the water surface, and the value of the velocity potential on that surface. An extremely wide range of initial conditions are possible, but here we report on results with an initially uniform wave train as described in the next section. For waves of initially gentle steepness linear theory is used, but accurate wave solutions are used for initial waves

of moderate steepness. We only consider the more interesting case where the internal waves and the surface waves have the same direction of propagation.

2.3. *Ray theory*

We also use ray theory to model the interaction of the short waves with the surface current due to the internal wave discussed above. The reader is referred to Crapper (1984) for details of ray theory in this context. In brief, ray theory assumes that at any particular point the solution surface locally looks like a periodic plane wave train and that any variations in the wave amplitude a, frequency ω and wavenumber k are slow, i.e. changes over one wavelength are small. Here, ω is the frequency in the (x, t) frame, so that the surface wave dispersion equation is

$$(\omega - Uk)^2 = gk \tag{3}$$

in the absence of surface tension effects. For examples with surface tension see Trulsen & Mei (1993). If we choose waves propagating in the positive direction initially and hence take the phase velocity $c = +(g/k)^{1/2}$ to be relative to the water moving with the current, the dispersion relation may be written as

$$c^2 = \frac{g}{\omega}(c + U). \tag{4}$$

The waves corresponding to $c = -(g/k)^{1/2}$ are not excluded since they also correspond to a root of (4); see below.

The assumption of small variation over one wavelength leads to equations which define lines in (x, t) which are characteristics of the system and are known as rays. In one dimension, the ray equation simplifies to

$$\frac{\mathrm{d}x}{\mathrm{d}t} = U(x) + c_g. \tag{5}$$

Here note that the $\mathrm{d}/\mathrm{d}t$ defines differentiation with respect to time along a ray and $c_g = c/2$ is the group velocity for waves in on deep water in the absence of a current. For a particular ray (4) defines the frequency, ω, by

$$\frac{\omega}{g} = \frac{c_1 + U(x_0)}{c_1^2}, \tag{6}$$

where x_0 is the position of the ray at time $t = 0$, and c_1 is the value of c at that point, which is constant for all rays.

The quadratic equation (4) gives two solutions for c:

$$c = \frac{g}{2\omega}\left(1 \pm \left(1 + \frac{4\omega U}{g}\right)^{1/2}\right). \tag{7}$$

The value of $\mathrm{d}x/\mathrm{d}t$ at $t = 0$ determines which root to take initially. However, most of the interesting wave patterns either occur for, or can be found with, waves that are travelling in the same direction as the internal wave. Hence we restrict initial conditions to the case with a positive sign, giving, at $t = 0$,

$$\frac{\mathrm{d}x}{\mathrm{d}t} = \tfrac{1}{2}c_1 + U(x_0). \tag{8}$$

If in the subsequent propagation of a ray $U + \frac{1}{2}c = 0$ then the wave is reflected relative to the (x, t)-plane. This corresponds to a transfer to the 'other' root of (7) for

c. This is discussed in Peregrine (1976). Note that in the figures showing ray paths a * indicates the point of reflection, x_{ref}, of individual rays.

In the earliest work on this system, Gargett & Hughes (1972), took ω to have a constant value over the whole wave field since this enables analytic solutions to be found. However this gives an atypical wave field. An example of rays for a solution of this form is given in figure 2. The initial phase speed, $c_0 = g/\omega$, of all the waves considered in the fixed frame of reference was taken to be unity, so all the rays have the same frequency. Figure 2 shows ray paths with $V = 0.245\,\text{m}\,\text{s}^{-1}$ and $U_c = 0.03\,\text{m}\,\text{s}^{-1}$ in a frame of reference moving with the internal wave. Initially, the rays shown are at equally spaced intervals. The region in space in which the rays propagate is determined from the condition that the roots of the quadratic equation for c, (7), are real, i.e. $1 + 4\omega U(x)/g \geqslant 0$. This implies that rays can propagate only when

$$\cos(Kx) \geqslant \frac{V}{U_c}\left(1 - \frac{c_0}{4V}\right). \tag{9}$$

Also, note that (7) demonstrates the effect of the current visible in figure 2; that is, the waves travel much faster with the current (to the right) than they do against the current (to the left).

In a computational study, we can choose any initial condition, but for simplicity we consider the short waves to be of constant wavenumber at $t = 0$, hence c_1 is the same for all rays. Although this may appear to be as special as taking ω constant, this is not so since a glance at the figures later in the paper shows that this condition leads to focusing of rays which is the generic behaviour for such hyperbolic systems. This initial condition is used since it is a representation of the waves that might be generated by a single gust of wind.

When the short-wave field is defined in this way, the system can be described by just three dimensionless parameters. Two velocity-ratio parameters θ and γ may be chosen as

$$\theta = \frac{U_c}{V} \quad \text{and} \quad \gamma = \frac{c_1}{V} = \left(\frac{g}{k_1}\right)^{1/2}\frac{1}{V}, \tag{10}$$

where k_1 is the wavenumber of the initial wave disturbance. The other parameter is the initial steepness, $a_1 k_1$ of the short waves. For linear theory, the amplitude, a_1, is just a simple multiplier.

3. Results

3.1. *A standard example*

Before beginning specific analysis, consider the physics of a general case. Figure 3 shows the streamline pattern due to the two-layer model discussed earlier. Note that this diagram is in the (x, y)-plane, i.e. the frame of reference is moving with the phase speed of the internal wave. In this frame of reference, the flow pattern is steady. The internal wave (at the density interface) and the surface are shown by heavy lines. The surface elevation due to the internal wave cannot be seen on this diagram due to its small slope. One wavelength of the internal wave is shown. Figure 3 indicates, intuitively, the effect the underlying internal wave may have on the set of short waves of initially constant wavenumber on the surface. The current acts to 'spread out' (decreasing wavenumber and steepness) the waves in region R_I and to 'bunch together' (increasing wavenumber and steepness) the waves in region R_{II}. We will

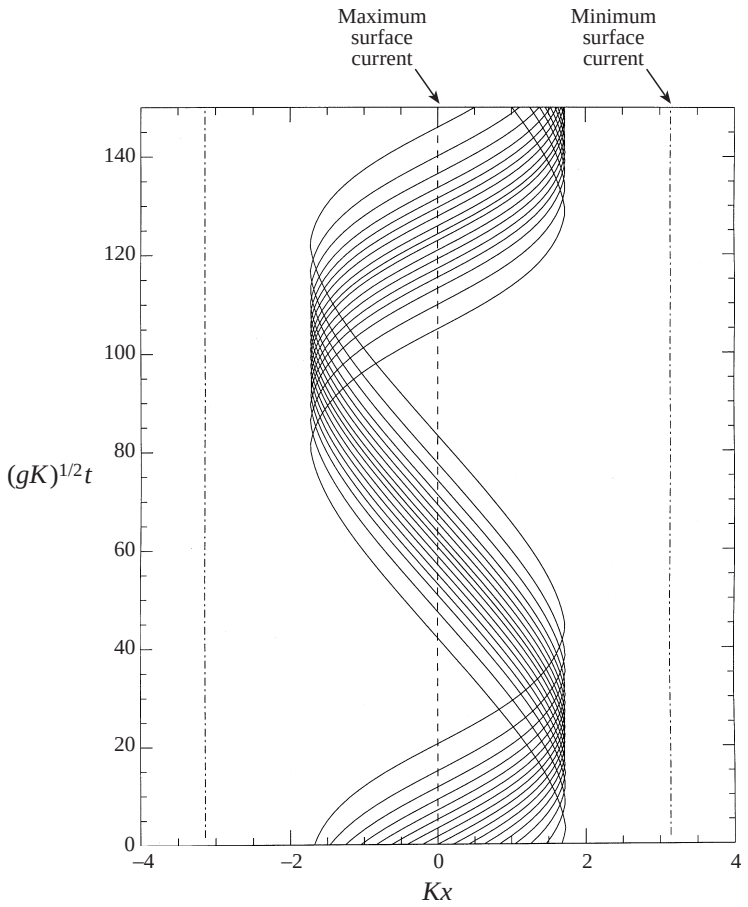

FIGURE 2. Ray diagram for waves of constant frequency, ω. The frame of reference is moving with the internal waves and rays start at $t = 0$ at equally spaced intervals.

demonstrate that this is only the case for sufficiently short waves with a moderate surface current.

Figure 4 shows surface profiles resulting from a fully nonlinear calculation. Time, t, non-dimensionalized with $(gK)^{1/2}$, is given on the ordinate axis and position, $\hat{x}$, on the abscissa, i.e. this is a fixed frame of reference. Two spatial wavelengths and more than one time period of the internal wave are shown. The maximum and minimum values of the surface current are indicated by dashed lines and dash-dot lines respectively. Regions R_I and R_{II} are also indicated. For these values of (θ, γ), we note that our intuitive idea of the 'spreading out' and 'bunching together' in time of the short waves by the internal wave is correct. Note: we show exceptions to this later.

It is physically relevant to consider up to several hundred short waves on one wavelength of an internal wave. We have taken for an example flow in an estuarine channel, as it is possible to obtain experimental data from situations of this type, with $\lambda = 0.4\,\mathrm{m}$ and $\Lambda = 120\,\mathrm{m}$ giving $\Lambda/\lambda = 300$. Here we could have a pycnocline with $h_1 = 6.0\,\mathrm{m}$ with density difference 2.5 parts per thousand say, and the surface current may be of around $0.04\,\mathrm{m\,s^{-1}}$. These physical values give (θ, γ)=(0.122, 2.416) and we hereafter refer to this as the 'standard case' (shown in figure 4).

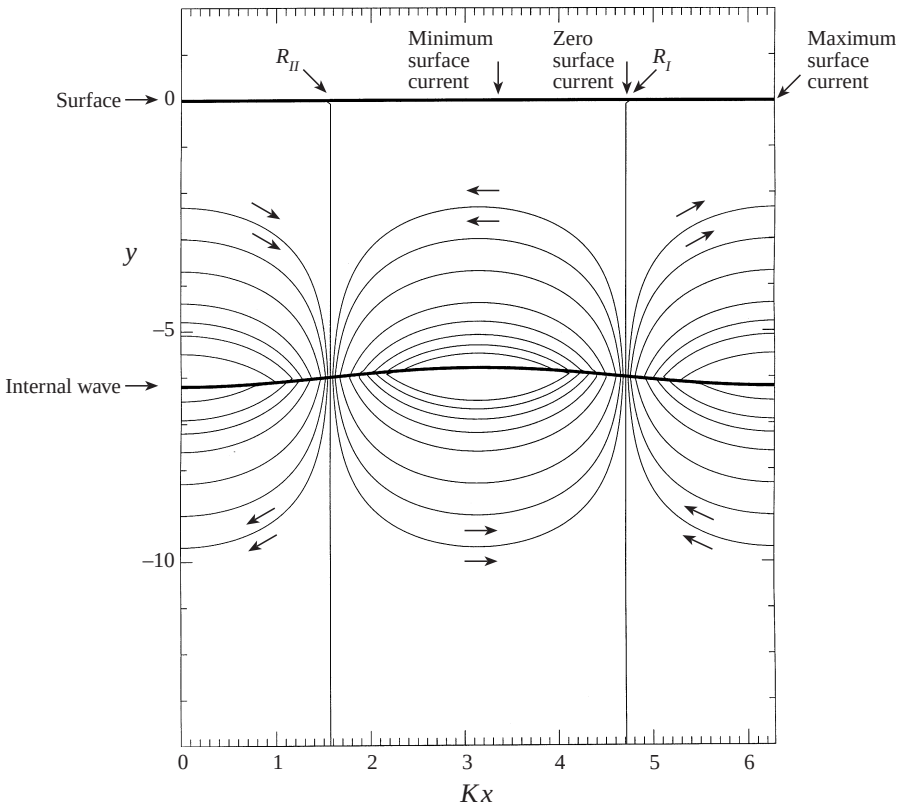

FIGURE 3. Streamlines for the two-layer internal-wave model.

As implied in the introduction, this work is not only applicable to internal waves on shallow pycnoclines as discussed above, but also to deeper thermoclines present in warmer oceans. In these regions, the density difference is slightly larger, although of the same order of magnitude, and internal waves may have wavelengths of many hundreds of metres. Currents may also be larger in magnitude. For example, results from the standard case are also applicable to the of interaction between an internal wave at a depth of 100 m with a wavelength of 500 m which generates a sinusoidal surface current of strength 0.230 m s^{-1} and phase speed of 0.990 m s^{-1} interacting with surface waves of initial wavelength 3.66 m, when the density difference is 2.8 parts per thousand.

It is computationally impractical to model hundreds of short waves in full detail. Therefore we take a smaller, but still large, number of short waves per wavelength of the internal wave, keep (θ, γ) at the same value and adjust the strength, U_c, and phase speed, V, of the current accordingly. The 20 short waves per wavelength of the internal wave shown in figure 4 seems to be a large enough number to demonstrate the focusing and steepening of the waves. The short waves have an initial steepness of $ak = 0.01$. Results here are shown with a vertical exaggeration of 40 : 1. If no internal wave were present then these would propagate steadily without any distortion since they are too gentle for the Benjamin–Feir instability to have an effect. However, the focusing by the internal wave causes them to steepen so that some of the waves are steep enough to be noticeably affected by nonlinearity, even though this case was originally chosen to represent the linear wave solution.

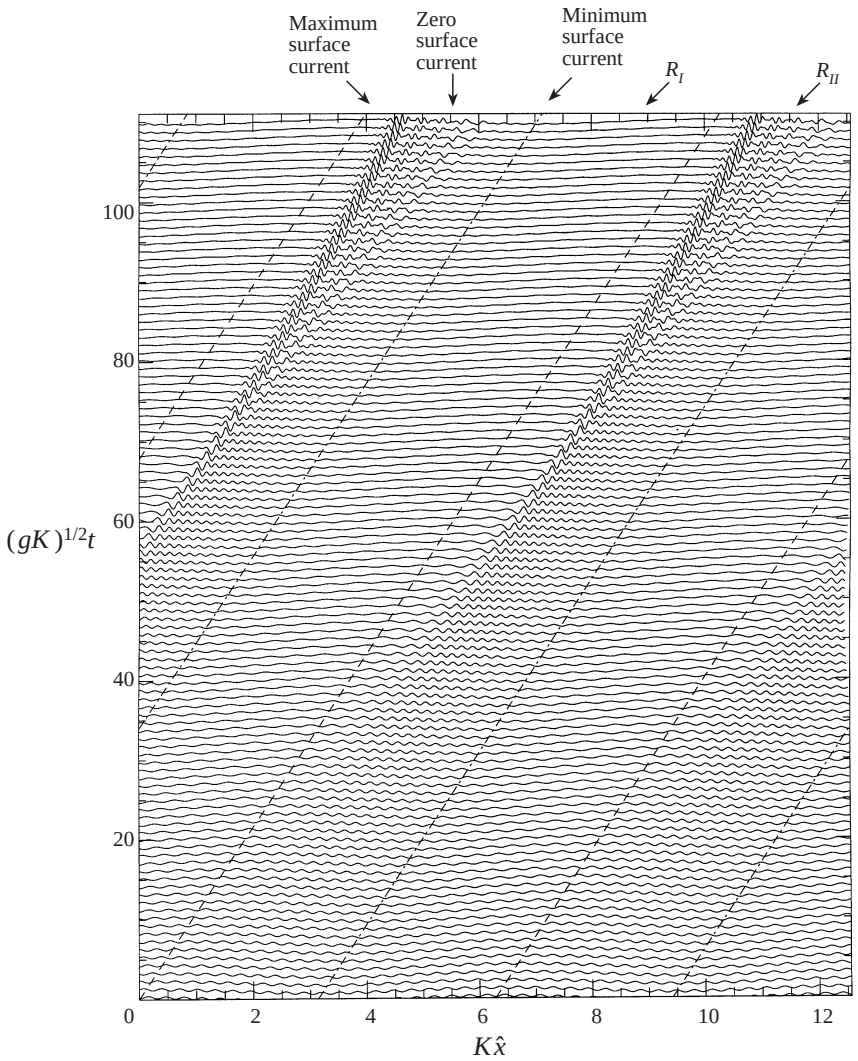

FIGURE 4. Fully nonlinear results: standard case. The frame of reference is fixed. Surface current $= U_c \cos(\hat{x} - 0.093t)$, $(\theta, \gamma) = (0.122, 2.416)$, initial steepness of 20 waves is $ak = 0.01$ and vertical exaggeration 40 : 1.

Figure 5 gives the corresponding ray diagram. The * indicate the points at which the rays are reflected. The position of the focus occurs when neighbouring rays first meet and here coincides with the point of reflection of the rays originating from $x_0 = 2n\pi$. As is generally the case, the focus is a cusp of two caustics. We see that regions of high concentration of rays in figure 5, e.g. leading up to the focus and along the left-hand caustic, correspond to relatively steep waves in figure 4. Similarly, there are very few rays in region R_I where the waves are much less steep. The irregular part of the wave pattern in figure 4 corresponds to the region between the caustics in figure 5 where three families of rays overlap.

We are interested in how the amplitude a and phase χ vary along a ray. The wave action A is related to amplitude a by $A = \frac{1}{2}\rho_1 c a^2$ in linear theory. It is conserved in the system as a whole, since we are ignoring dissipation, and the variation can be

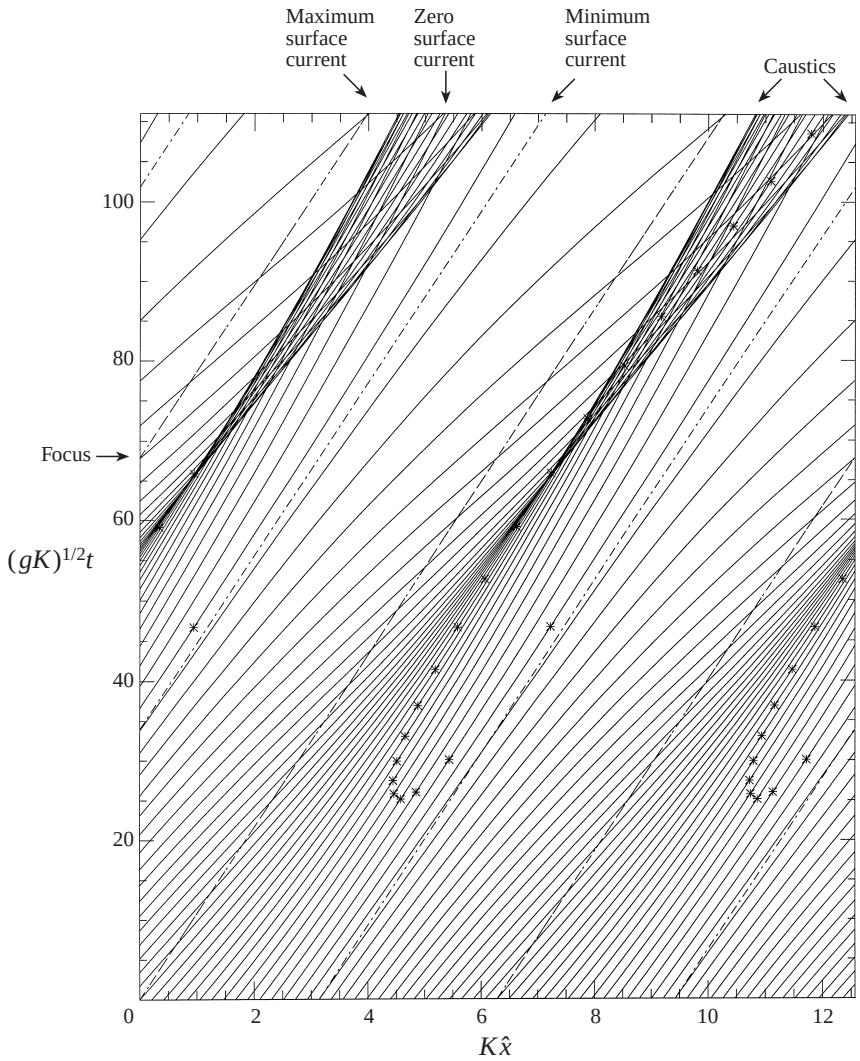

FIGURE 5. Ray diagram: standard case. The frame of reference is fixed. Surface current = $U_c \cos(\hat{x} - 0.093t)$ and $(\theta, \gamma) = (0.122, 2.416)$.

described by

$$\frac{\mathrm{d}A}{\mathrm{d}t} = -A\frac{\partial}{\partial x}\left(U(x) + \tfrac{1}{2}c\right), \tag{11}$$

where $\mathrm{d}/\mathrm{d}t$ is again differentiation along a ray. Similarly the phase, $\chi = kx - \omega t$ varies with

$$\frac{\mathrm{d}\chi}{\mathrm{d}t} = \tfrac{1}{2}(\omega - Uk) = -\frac{g}{2c} \tag{12}$$

for a steady, slowly varying current; this can be shown by direct differentiation of the phase, along a ray. Once again, for further details on the method of ray tracing see Crapper (1984).

As mentioned in § 1, ray theory breaks down with a singularity of A at the focus and the caustics. When presenting the ray-theory wave picture, we take the simple step

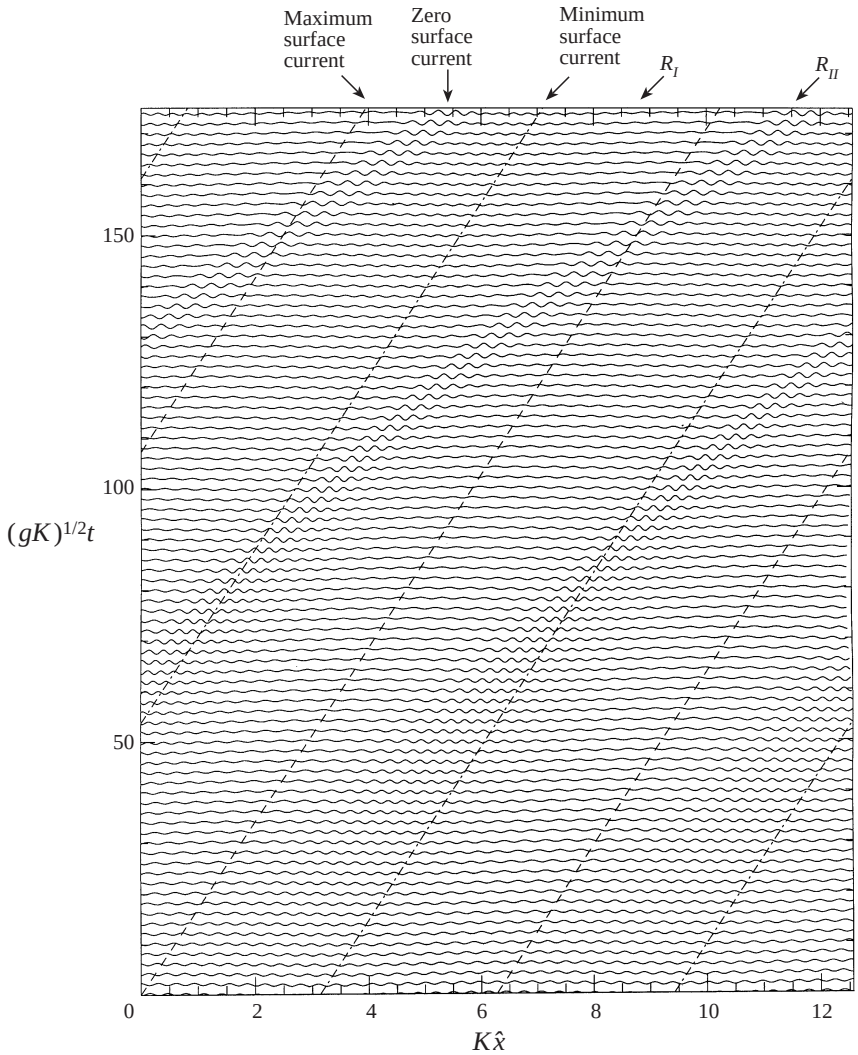

FIGURE 6. Fully nonlinear results: 'longer' short waves. The frame of reference is fixed. Surface current $= U_c \cos(\hat{x} - 0.059t)$, $(\theta, \gamma) = (0.122, 3.821)$, initial steepness of 20 waves is $ak = 0.01$ and vertical exaggeration 40 : 1.

of omitting values where the amplitude exceeds an arbitrary critical value rather than calculate the appropriate uniform approximation (see for example figure 10 where linear ray theory results are given by the dotted line). This gives discontinuities in the surface profile in the region leading up to the focus and at the caustics there is a sharp unphysical change in wave form. Higher-order dispersive effects which can be incorporated to make a uniform non-singular approximation are not discussed here since we wish to assess the simplest theory, and, as may be seen, the present results cover almost all the wave field.

3.2. *Two other cases: 'longer' short waves and stronger current*

As mentioned in § 2, we are interested in the effect of varying the initial length of the short waves and the strength of the current due to the internal wave, which

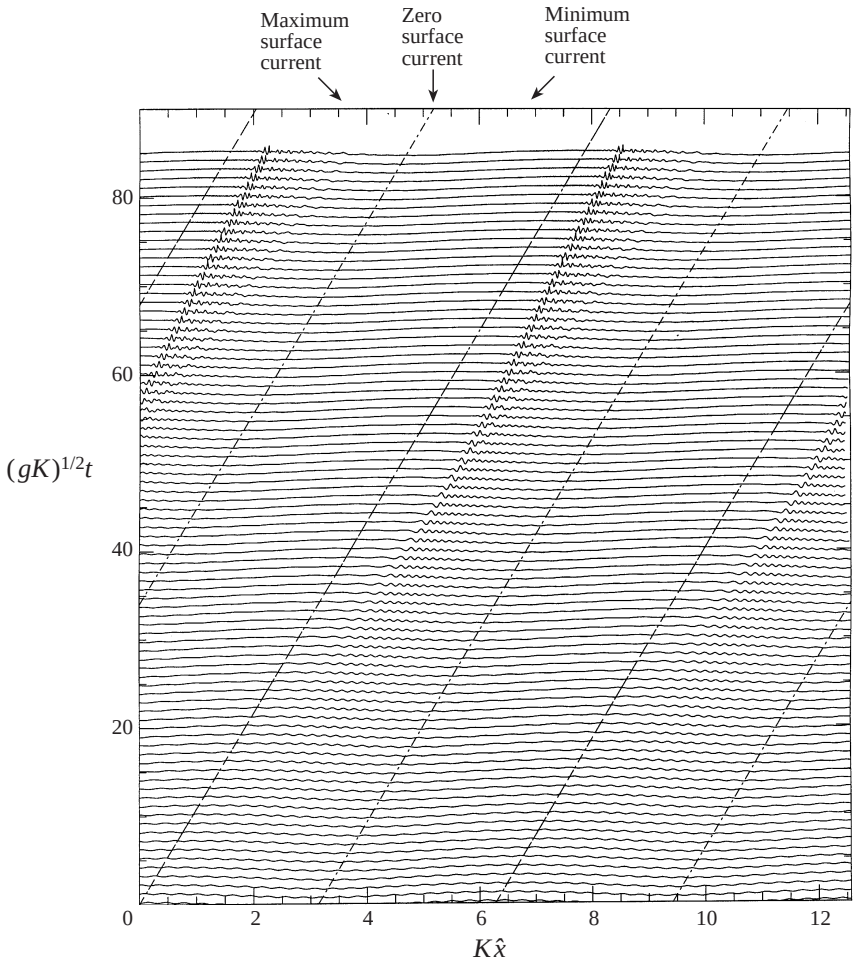

FIGURE 7. Fully nonlinear results: stronger current. The frame of reference is fixed. Surface current $= U_c \cos(\hat{x} - 0.059t)$, $(\theta, \gamma) = (0.245, 2.416)$, initial steepness of 20 waves is $ak = 0.01$ and vertical exaggeration 20 : 1.

corresponds to varying γ and θ respectively. We consider initially 'longer' short waves by taking $\lambda = 1.00\,\mathrm{m}$, keeping Λ, U_c, and V constant, so $\Lambda/\lambda = 120$ and $(\theta, \gamma) = (0.122, 3.821)$. Note that nonlinear calculations still have 20 short waves per wavelength of the internal wave, with the other parameters adjusted accordingly, as discussed for the standard case. Similarly, we double the strength of the current to $U_c = 0.08\,\mathrm{m\,s^{-1}}$, keeping λ, Λ, and V as for the standard case which gives $(\theta, \gamma) = (0.245, 2.416)$. Figures 6 and 7 show the effect of increasing γ and θ respectively with nonlinear computations. These calculations start with short waves of initial steepness $ak = 0.01$ (as in figure 4 for the standard case). Note that figure 6 is shown with a vertical exaggeration of 40 : 1 whereas figure 7 is shown with a vertical exaggeration of 20 : 1.

After an initial focusing, 'longer' short waves are less influenced by the underlying internal wave. A wave packet then forms which is wider than for the standard case, and waves are less steep. There is little change in the form of the wave packet as it passes over the crests and troughs of the internal wave. The ray diagram which

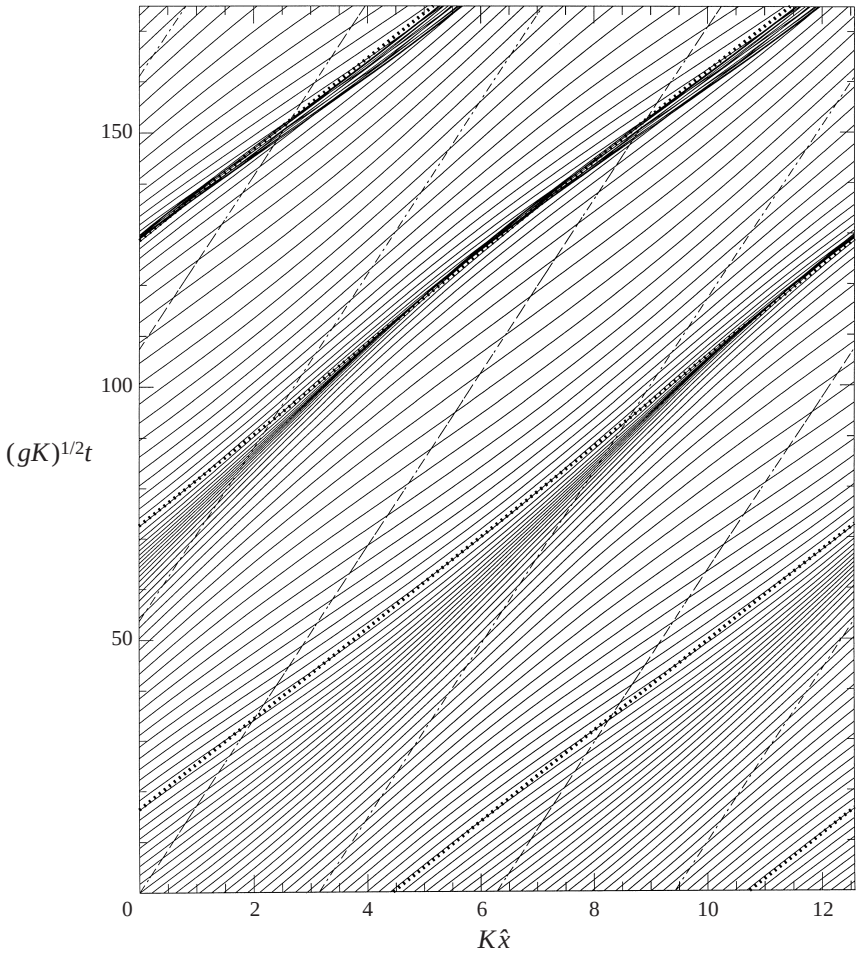

FIGURE 8. Ray diagram: 'longer' short waves. The frame of reference is fixed. Surface current $= U_c \cos(\hat{x} - 0.059t)$ and $(\theta, \gamma) = (0.122, 3.821)$, $\cdots$ is the asymptotic approximation given by (25).

corresponds to figure 6 is shown in figure 8. This shows that the formation and propagation of the wave packet is also predicted by linear theory. 'Longer' short waves are discussed further in § 6.

The effect of increasing the current is to increase the range of steepness of the waves. Even when starting with 20 waves of steepness $ak = 0.01$, this stronger current causes the waves to steepen so much that they break at $t \sim 72$ with the usual computational tolerance parameters, compared to the maximum steepness achieved by the waves in the standard case of $ak = 0.122$. Also, the focusing of the waves occurs earlier for an increased current. Surface profiles shortly before breaking are shown without any vertical exaggeration in figure 9. Note that only one quarter of a wavelength of the internal wave is in this view. Also, due to the increased wave steepness tighter accuracy parameters are chosen to resolve more detail and the calculation progressed up until $t \sim 84.9$. This sensitivity to the numerical parameters is due to the modulation of the waves, and has a physical origin. Since phase and group velocities differ, individual waves move through any modulation, such as occurs through focusing or near a

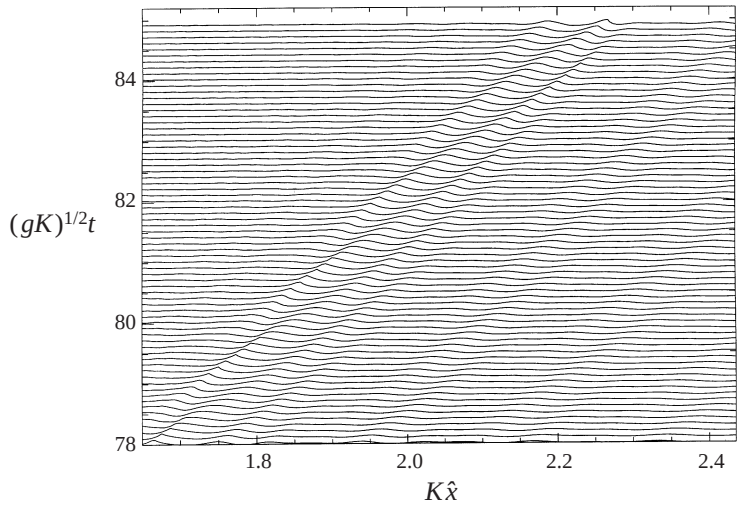

FIGURE 9. Final stages of wave breaking from figure 7: no vertical exaggeration. Surface current $= U_c \cos(\hat{x} - 0.093t)$, $(\theta, \gamma) = (0.245, 2.416)$ and initial steepness of 20 waves is $ak = 0.01$.

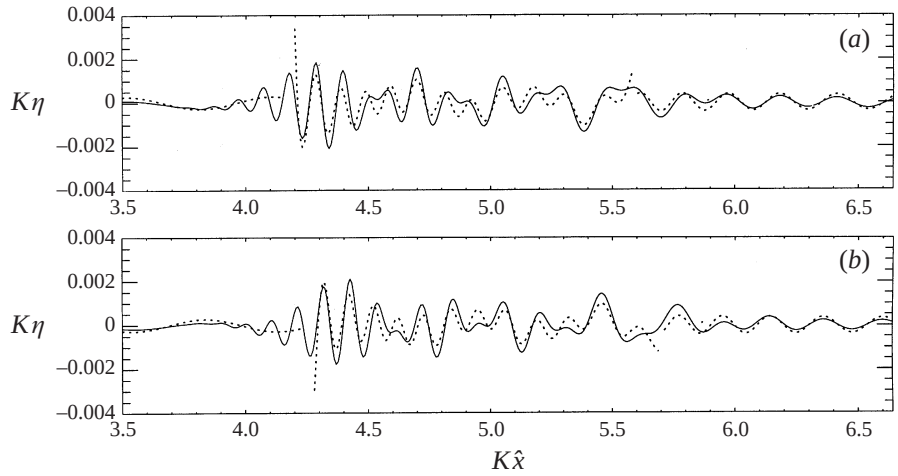

FIGURE 10. Comparing linear ray theory (· · · ·) and 'linear' results from the fully nonlinear potential solver (——): standard case. Surface current $= U_c \cos(\hat{x} - 0.093t)$, $(\theta, \gamma) = (0.122, 2.416)$, initial steepness of 20 waves is $ak = 0.005$: (*a*) $t = 106$, (*b*) $t = 107$.

caustic. When a wave crest is at the peak of a modulation that is growing, it might just break. However, with a slightly earlier arrival at the peak, it might just miss breaking, and then the breaking is delayed, by a wave period for the case of deep water waves.

4. Nonlinearity, steepness and wave breaking

We compare ray-theory results to 'linear' results from the fully nonlinear potential solver, i.e. for waves which are not steep enough for us to see nonlinear effects, say maximum ak less than about 0.1. For the standard case, we find slight differences in regions close to the focus and between the caustics. Just before the focus, the linear ray theory predicts unphysically large values for the wave amplitude.

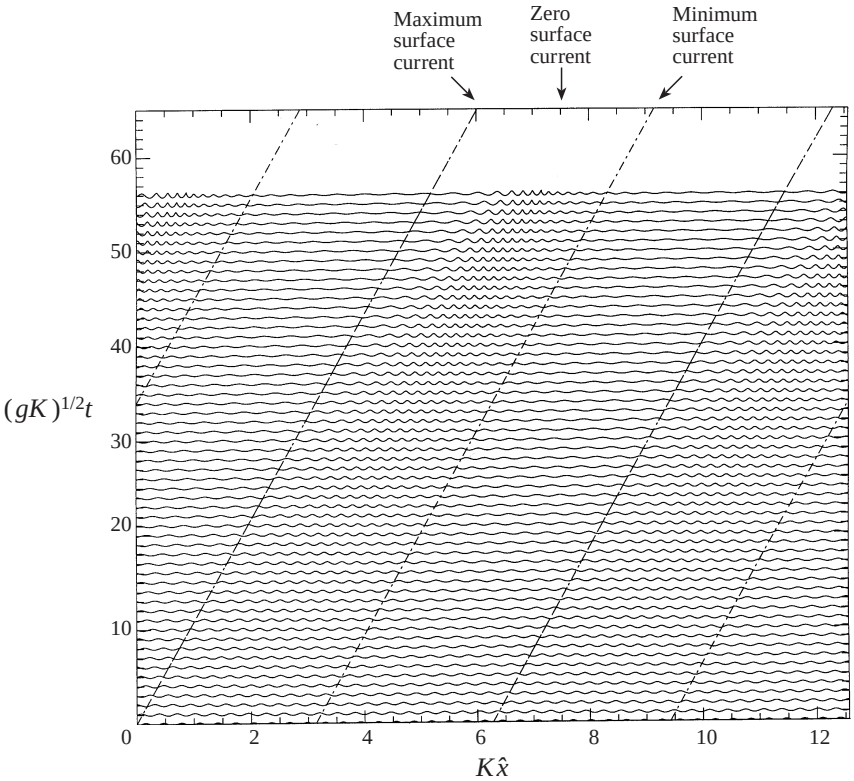

FIGURE 11. Steeper fully nonlinear results – computation stops due to wave breaking: standard case. Surface current $= U_c \cos(\hat{x} - 0.093t)$, $(\theta, \gamma) = (0.122, 2.416)$, initial steepness of 20 waves is $ak = 0.10$ and vertical exaggeration 4 : 1.

Figure 10 shows half a wavelength of the internal wave and compares results from the linear ray theory (dotted line) and 'linear' results from the fully nonlinear potential solver (full line) in order to make detailed comparisons, showing the wave surface between the caustics at times (*a*) $t = 106$ and (*b*) $t = 107$. We do not expect to see any nonlinear effects in the results from the nonlinear code, as steepnesses did not exceed 0.05 in the calculation; however, discrepancies are apparent. In each of parts (*a*) and (*b*), the waves do tend to be in the same place for both realizations. Outside the caustics, the ray theory waves are steeper than results from the full solution, whereas between the caustics in general the opposite is true. If we were expecting nonlinear effects to be apparent, we would explain this by self-focusing. However, as we do not expect to see any nonlinear effects, we are unable to explain this phenomenon. The ray theory does not predict the small waves shown just outside the left-hand caustic, although if we were to match together the linear results to obtain a continuous solution using an Airy function modulating the waves, as in, for example, Peregrine (1976), the results would include these short waves decaying in amplitude just outside the caustic position.

Figure 11 shows the fully nonlinear results for the standard case as in figure 4 but starting with waves ten times steeper. This is perhaps a more likely physical situation. The computation stops at $t \sim 56$ due to breaking. This is before the focus occurs.

Figure 12 compares the effects of varying steepness in more detail. Here results are presented with the internal-wave surface profile removed, since with the less steep

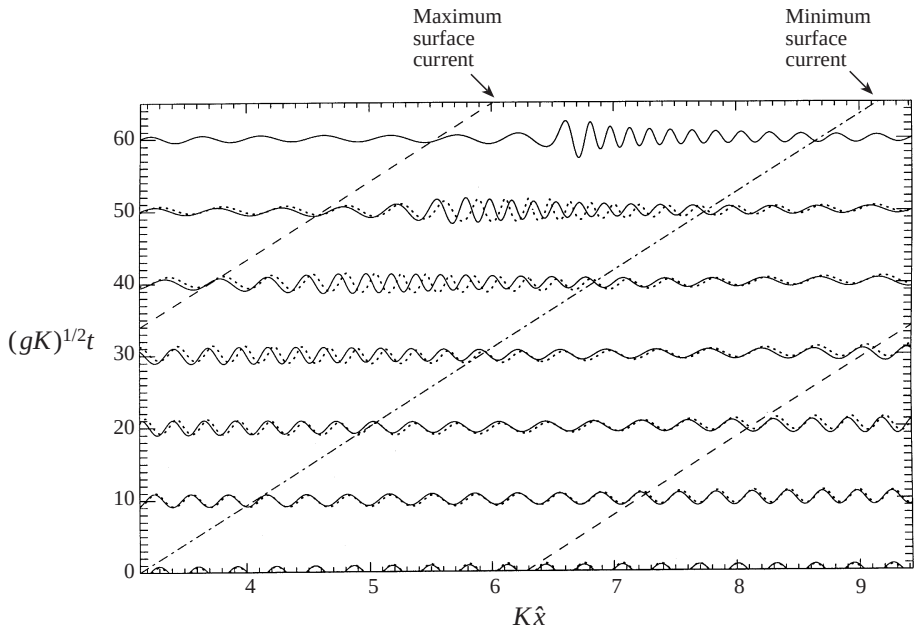

FIGURE 12. Comparing nonlinear steepness results: standard case. Surface current $= U_c \cos(\hat{x} - 0.093t)$, $(\theta, \gamma) = (0.122, 2.416)$: ——, $ak = 0.01$ initially (vertical exaggeration 100 : 1) and · · · ·, $ak = 0.10$ initially (vertical exaggeration 10 : 1).

waves having a vertical exaggeration which is ten times greater, the comparison would be confused if it were included. The main feature demonstrated here is that steeper waves travel faster. This can be seen to a greater extent in the regions where the internal wave has focused the short waves causing them to steepen (close to the focus and between the caustics) and decrease in wavenumber, and to a lesser extent away from these regions.

The nonlinear computations stop when the waves are 'about to break'. This really means that there are insufficient points in the regions of high curvature to give results which are within the accuracy required. As well as including normal breaking where the crest overturns, this lack of resolution also occurs if the wave approaches Stoke's limiting shape with a 120° slope at the crest. These regions of high curvature are of interest with respect to specular radar scattering and therefore we again would like to know the effect that varying θ, γ and the initial steepness has on the time and position of the breaking waves. We take the three cases (standard, 'longer' short waves and stronger current) and vary the initial steepness of the short waves to see how it affects the time and position at which breaking occurs. Figure 13 shows the results obtained. The $\times$ indicate the points from calculations. The results are accurate to one non-dimensional unit of time.

However, although results from the nonlinear calculations are accurate to a high degree, the actual condition for the computation to stop is very sensitive to the computational parameters, as discussed above. This is demonstrated in figure 14 where, with two calculations subject to the same accuracy parameters, 'breaking' occurred first at $t = 92$, and then, when output was required every half time unit, giving a small change to the time stepping, it progressed to $t = 94$. The results from the latter calculation are shown, but it is clear that at $t = 92$ the wave on the

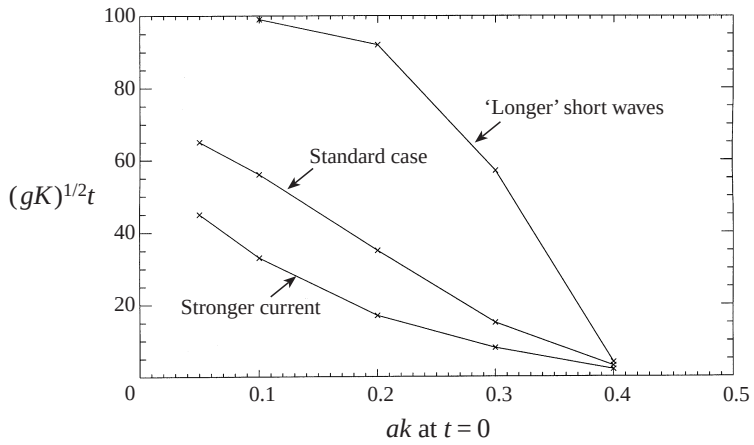

FIGURE 13. Time of breaking against initial steepness of the short waves.

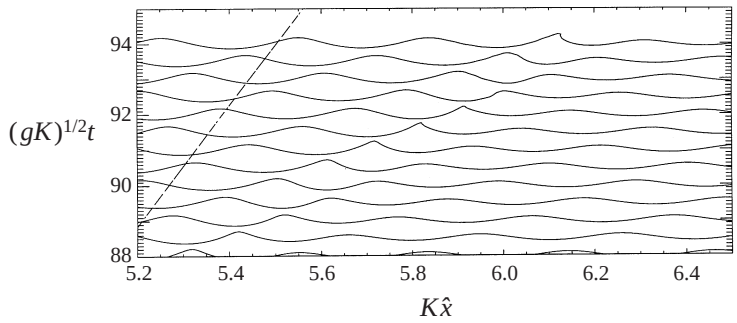

FIGURE 14. Last steps of a 'longer' short-wave calculation, with $ak = 0.20$ initially.

far right-hand side of the group is close to breaking. Given this sensitivity to the computational parameters, times given for breaking should not be taken as precise as a difference of two periods readily occurs.

Regular waves on deep water break when their steepness exceeds approximately $ak = 0.43$, which corresponds to the maximum value of the total energy and the impulse of the wave (see Tanaka 1983 for further discussion). This explains the short time to breaking for all three cases when $ak = 0.40$ initially. Note: accurate nonlinear waves are used for the initial conditions for this part of the study.

Figure 13 shows that under the same initial conditions, a stronger current decreases the time for breaking to occur whereas 'longer' short waves take longer to break. The time to breaking is related to the time at which focusing occurs, which is found from linear ray theory. (This is discussed in more detail in the next section.) It is also interesting to consider the time of breaking relative to the time at which focusing occurs. This is shown in figure 15. In all cases shown here, the breaking occurs before or at the focus due to the steepening of the waves caused by the focusing effect of the internal wave. However, this is not always the case, e.g. figure 7 shows breaking after the focus when starting with waves of steepness just $ak = 0.01$. Also, when starting with waves of steepness $ak = 0.05$, the 'longer' short waves do not break, even after focusing.

Figures 9 and 16 shows the final stages up to wave breaking for the stronger current

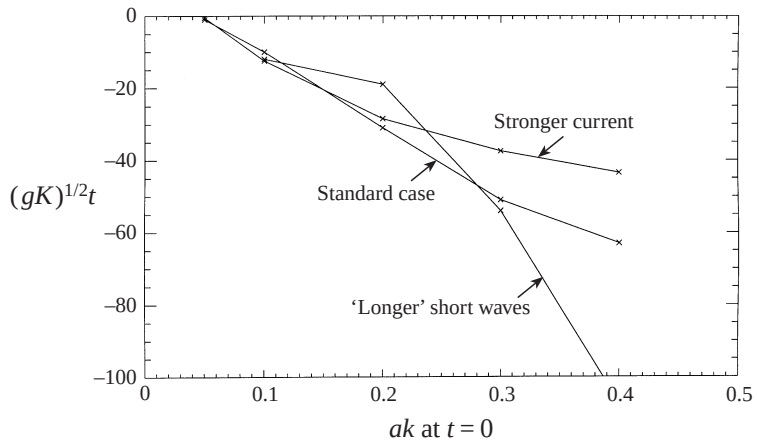

FIGURE 15. Time of breaking relative to the time at which focusing occurs (predicted by linear ray theory) against initial steepness of the short waves.

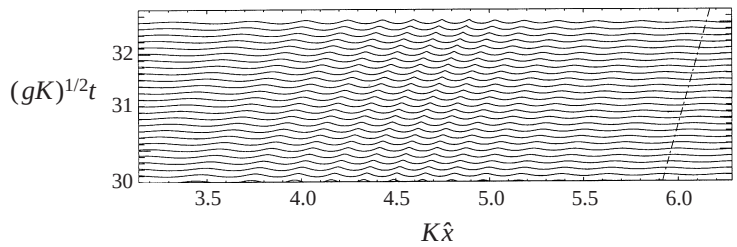

FIGURE 16. Final stages of wave breaking with a stronger current: no vertical exaggeration. Surface current $= U_c \cos(\hat{x} - 0.093t)$, $(\theta, \gamma) = (0.245, 2.416)$ and initial steepness of 20 waves is $ak = 0.10$.

with different initial steepnesses and no vertical exaggeration, with only a portion of the internal wave shown. Breaking occurs in a group of steep short waves (to which the radar may be sensitive) between larger regions of less steep waves. The sun glitter in figure 1 is related either to such steep waves, or to even shorter waves on them. We note that the surface pattern does not change much when the waves are about to break. At some point, a wave crest in the group of steep waves becomes steep enough to break. The number of waves in the group differs considerably between the two cases, and the breaking event appears stronger in figure 9, when breaking occurred after the focus.

The detail of breaking is similar to that which occurs in the absence of currents when the Benjamin–Feir instability triggers self-focusing and wave groups steepen (see, for example, Dold & Peregrine 1986). For the applications we envisage, with many more short waves, the self-focusing of steep waves may be more important. This is being investigated further.

5. Linear ray theory: analytical solutions

5.1. *Focusing*

Adjacent ray paths which are solutions of (4) and (5) subject to the initial conditions described above meet to form caustics and foci. In regions where the rays meet, the ray theory breaks down as the corresponding wave amplitude becomes singular. In

practice, higher-order dispersion and/or nonlinear effects come into play which can result in smooth solutions if the waves are not too steep.

As discussed in Berry (1981), the intuitive way to think of caustics and foci is to consider a perturbation of the initial conditions and find a position (x_r, t_r) on a ray in the (x,t)-plane for $t > 0$ where the rays coincide. From (5) we have

$$t_r = \int_{x_0}^{x_r} \frac{1}{U + c/2} \mathrm{d}x \tag{13}$$

to describe a ray before reflection, i.e. before $U + c/2 = 0$, where integration is along a ray. Although on first sight it would seem that consideration of the integrand in (13) close to reflection would lead to problems, as we are integrating along a ray, we find that as $U + c/2 \to 0$, $\mathrm{d}x \to 0$ and then changes sign. So the equations remain well behaved in these regions. Differentiating (13) with respect to x_0 in order to get the ray envelope, we obtain

$$\frac{\partial t_r}{\partial x_0} = \int_{x_0}^{x_r} \frac{\partial}{\partial x_0} \left(\frac{1}{U + c/2} \right) \mathrm{d}x + \frac{\partial x_r}{\partial x_0} \left[\frac{1}{U + c/2} \right]_{x=x_f} - \left[\frac{1}{U + c/2} \right]_{x=x_0}. \tag{14}$$

In the special case of a perfect focus, i.e. the position, x_f, and the time, t_f, at which the rays meet is independent of their initial position x_0, then the above equation simplifies to

$$\left[\frac{1}{U + c/2} \right]_{x=x_0} = \int_{x_0}^{x_f} \frac{\partial}{\partial x_0} \left(\frac{1}{U + c/2} \right) \mathrm{d}x. \tag{15}$$

The time, t_f, at which the rays meet is obtained from the numerical integration of (13).

5.2. *Linear and quadratic currents*

As we have not found an analytic solution to (13) and (14) for a sinusoidal current, we have investigated approximate solutions by using suitable algebraic forms for $U(x)$. Two approaches have been taken to investigate the time and position of the caustics/foci. One is to solve (5) to find the ray paths and the other is to attempt to solve (14) to find (x_r, t_r).

Considering a truncated linear Taylor expansion about any point $Kx \in [-\pi, \pi]$ gives an algebraic approximation for the current at that point. The most sensible point at which to consider a linearly varying current, $U(x) = -ax - b$ where $a, b > 0$, is at the point of inflection of $U(x)$ where there is no quadratic term in the expansion, i.e. at $Kx = \pi/2$ giving $U(x) = -U_c K x - (V - U_c \pi/2)$. Figure 17 shows ray paths on a linearly varying current in the (x,t)-plane, i.e. the frame of reference is moving with speed V. This form of current gives a linear relationship between x_0 and the position of reflection of the rays x_{ref}. In this case, solving (5) explicitly leads to an equation for the ray paths before reflection occurs:

$$x = -\frac{1}{a} \left\{ b + T \left[\gamma V T + U(x_0) T - \gamma V \right] \right\}, \tag{16}$$

where $T = \mathrm{e}^{-at/2}$. Consideration of these ray paths shows that rays do not meet and no caustics or foci form. Thus, the analysis shows that on a linearly varying current, neighbouring rays never meet for this uniform-wavenumber initial condition.

Considering a quadratic truncated Taylor expansion for $U(x)$ about its maximum value at $x = 0$ gives a quadratic form for the current, $U(x) = -ax^2 - b$, where $a, b > 0$. Here $a = U_c K^2/2$ and $b = V - U_c$. Figure 18 shows the ray paths using this form for

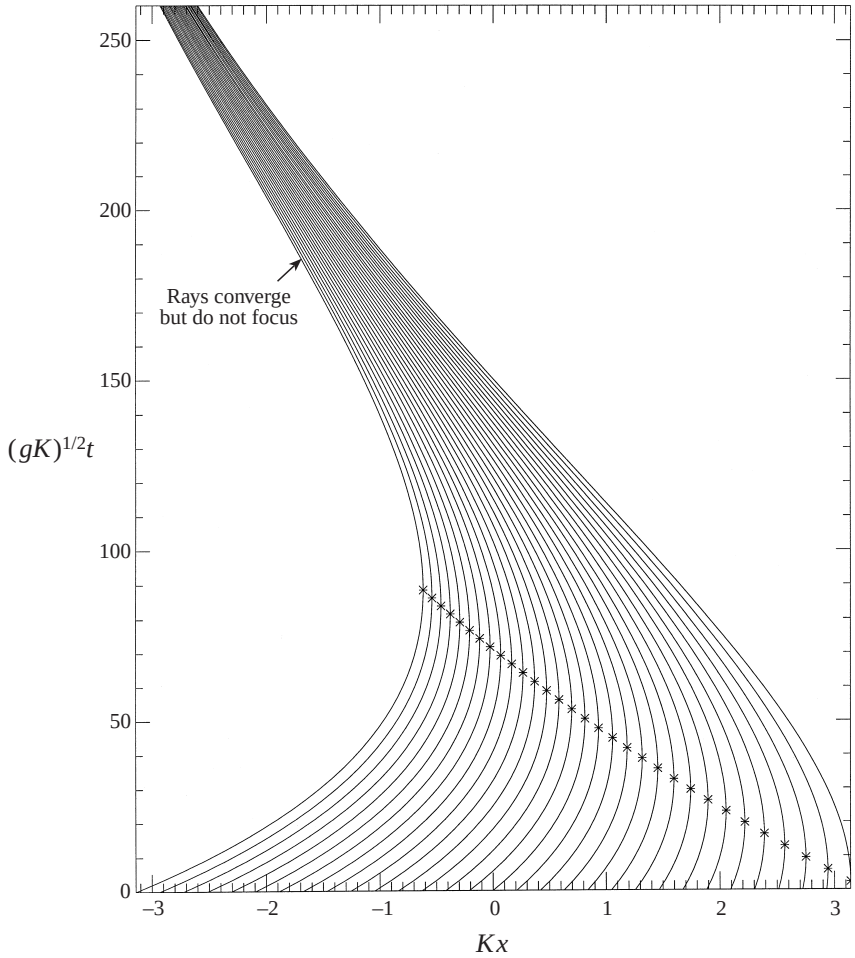

FIGURE 17. Rays for an initially uniform wave field on a current $U(x) = -ax - b$, where $a = U_c K$, $b = V - U_c\pi/2$ and $U_c/V = 0.122$. The frame of reference is moving with speed V.

$U(x)$ and we see that all the rays focus at one point: a perfect focus. The dashed line indicates the position of maximum current. Equation (5) can be solved explicitly to give an equation for the ray paths before reflection occurs:

$$t = -\frac{1}{(ab)^{1/2}}\,[\arctan(\sinh(q \pm Q))]_{q_0}^{q}\,, \tag{17}$$

where Q and q are defined by $\tanh Q = (1 - 4\omega b/g)^{1/2}$, $\tanh q = ((g - 4\omega(ax^2 + b)/(g - 4\omega b))^{1/2}$ and q_0 is q evaluated at $x = x_0$. The two solutions correspond to $\mathrm{d}x/\mathrm{d}t > 0$ and $\mathrm{d}x/\mathrm{d}t < 0$ at $t = 0$ respectively. As this quadratic current gives a perfect focus, it is simpler to work with (15). This leads to

$$x_{\mathrm{f}}^2 = \frac{1}{4a}\frac{(\gamma V - 2b)^2}{(\gamma V - b)} \tag{18}$$

which, as expected, is independent of x_0, the initial position of the rays. It turns out that this is also the exact point of reflection for the ray starting from $x_0 = 0$. This is relevant to the general problem.

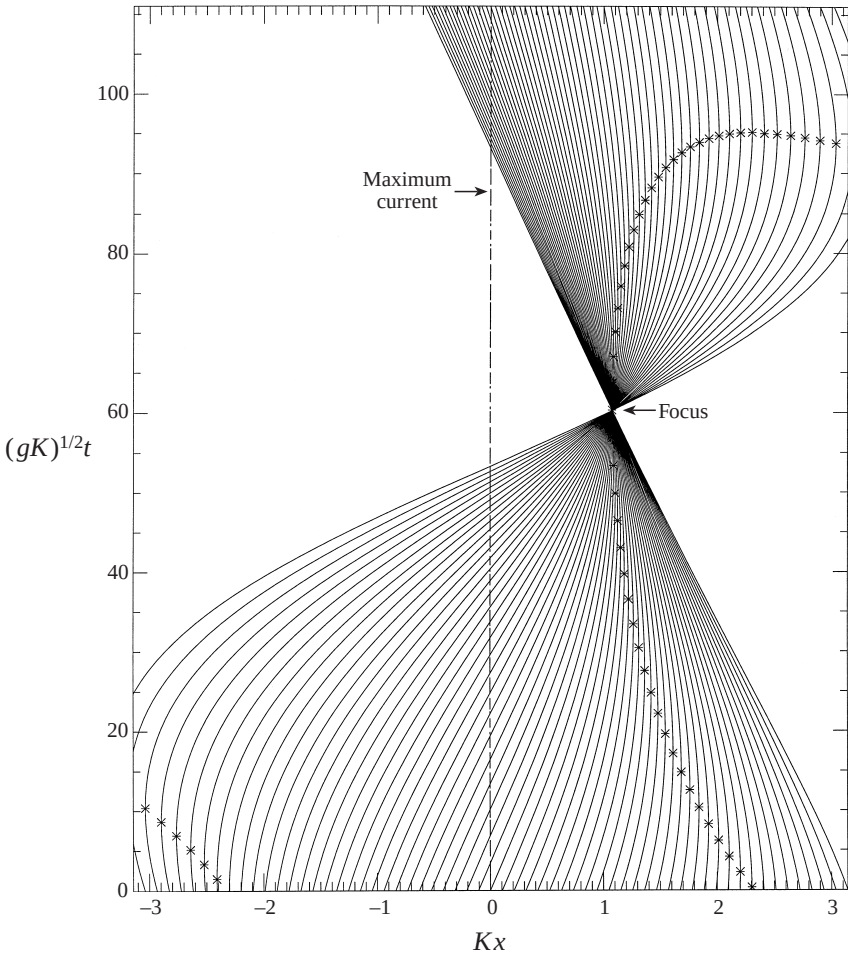

FIGURE 18. Rays for an initially uniform wave field on a current $U(x) = -ax^2 - b$, where $a = U_c K^2/2$, $b = V - U_c$ and $U_c/V = 0.122$. The frame of reference is moving with speed V.

5.3. *Velocity-ratio parameter space*

Results for reflection of rays on a sinusoidal current can be summarized in the parameter space of the two velocity ratios θ and γ defined in (10). Figure 19 shows the (θ, γ) parameter space for $0 \leqslant \theta \leqslant 0.4$ and $1 \leqslant \gamma \leqslant 5$. It is possible to predict whether or not a ray starting from $x = x_0$ will reflect by considering if there are solutions of $\mathrm{d}x/\mathrm{d}t = 0$. If we define

$$h(\theta, \gamma, Kx_0) = \frac{1}{\theta}\left(1 - \frac{\gamma^2}{4(\gamma + \theta\cos(Kx_0) - 1)}\right) \tag{19}$$

then this condition reduces to an investigation of whether there exist values of $x = x_{\mathrm{ref}}(x_0)$ which satisfy

$$\cos(Kx_{\mathrm{ref}}(x_0)) = h(\theta, \gamma, Kx_0). \tag{20}$$

We only consider values of (θ, γ) such that $\gamma > \theta + 1$ (corresponding to insisting $\omega > 0$ which fits in with the physical ranges of current, wavelengths etc. that we are considering). As would be expected from consideration of (6) given the even nature

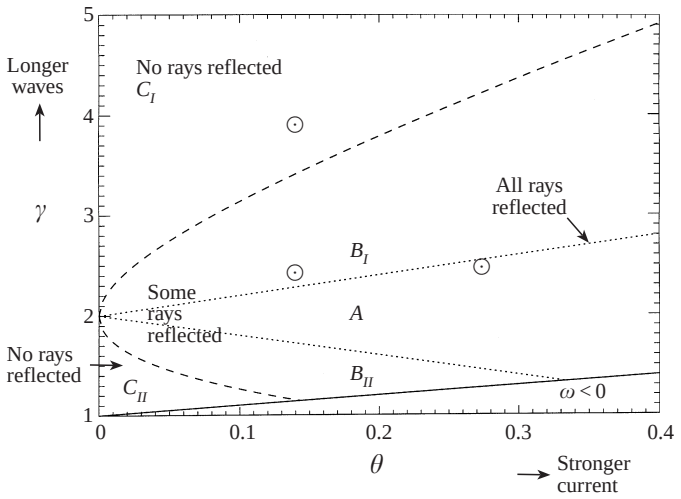

FIGURE 19. Different regimes for wave reflection in (θ, γ) parameter space for initially uniform waves. The $\odot$ indicate the positions in parameter space of the three cases considered in §§ 3 and 4; that is, (θ, γ)=(0.122,2.416), (0.122,3.821) and (0.245,2.416).

of the current, rays originating from equidistant points either side of $x_0 = 0$ have the same frequency ω and therefore reflect at the same position in space (in the frame of reference moving with current). However, they will reflect at different times owing to their different initial positions.

For $\gamma > 2(1+\theta)$ (regions with suffix I in figure 19), all rays propagate to the right initially in the frame of reference moving with the phase speed of the internal wave, i.e. $U + c/2 > 0$ at $t = 0$. Similarly, if $\gamma < 2(1-\theta)$ initially (regions with suffix II in figure 19) then all rays initially propagate to the left, i.e. $U + c/2 < 0$ at $t = 0$. In region A, where $2(1-\theta) < \gamma < 2(1+\theta)$, some rays propagate to the right and some to the left initially. In this region if we define $\chi = \cos^{-1}((1-\gamma/2)/\theta)$ where $\chi \in [0, \pi]$, then initially rays will propagate to the right if $Kx_0 \in (-\chi, \chi)$ and to the left otherwise.

The solutions of (20) are given by

$$Kx_{\text{ref}}(x_0) = \pm\cos^{-1}\left[\frac{1}{\theta}\left(1 - \frac{\gamma^2}{4(\gamma + \theta\cos(Kx_0) - 1)}\right)\right]. \tag{21}$$

If $\gamma/2+\theta\cos(Kx_0)-1 > 0$ then the positive root is taken and if $\gamma/2+\theta\cos(Kx_0)-1 < 0$ then the negative root is taken. This again corresponds to the initial direction of propagation of the rays.

The maximum value of $h(\theta, \gamma, Kx_0)$ occurs when $Kx_0 = 0$ and the minimum occurs when $Kx_0 = \pi$. It is possible to show that $h(\theta, \gamma, 0) \leqslant 1$ and that $h(\theta, \gamma, \pi) < -1$ in the domain we are considering unless $\gamma = 2(1+\theta)$. This means that all rays will reflect if and only if $\gamma = 2(1+\theta)$.

No rays will reflect if $h(\theta, \gamma, 0) < -1$. This is satisfied when either

$$\gamma > 2((1+\theta) + (2\theta(\theta+1))^{1/2}) \quad \text{(region } C_I\text{)} \tag{22}$$

or

$$\gamma < 2((1+\theta) - (2\theta(\theta+1))^{1/2}) \quad \text{(region } C_{II}\text{)}. \tag{23}$$

The cases considered in §§ 3 and 4 have been indicated on the (θ, γ) parameter

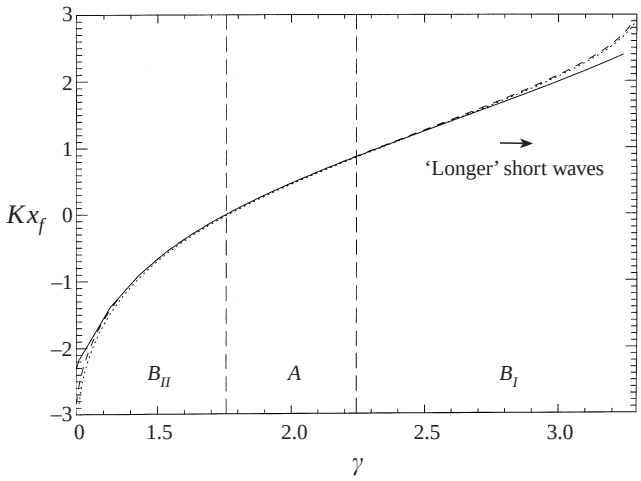

FIGURE 20. Ray-theory prediction of position of focus against γ for $\theta = 0.122$: numerical results (———), quadratic approximation ($\cdots$) and point of reflection of the $x_0 = 0$ ray (- - - -).

space diagram. The 'standard case' is in region B_I; that is, all rays initially propagate to the right when considered in a frame of reference moving with the phase speed V of the internal wave. This can be seen on figure 5 by comparing the gradients of the rays at $t = 0$ with the dashed lines which indicate the maxima and minima of the surface current. The next case of 'longer' short waves lies in region C_I were the rays never reflect. The final stronger current situation is just inside region A, very close to the line $\gamma = 2(\theta + 1)$ which is the condition required for all rays to be reflected. So most of the rays in this case will be reflected except for those initiating close to $Kx_0 = \pi$.

6. Predictions for the time and position of focusing on the internal wave

6.1. *Comparison with the quadratic current*

Figure 20 compares the position of the focus from the full numerical solution of (5) to the exact focusing of the quadratic solution in the frame of reference moving with the internal wave, for θ fixed at the 'standard case' value of 0.122 and γ varied over regions B_I, B_{II} and A of the velocity-ratio parameter space. We see that the quadratic approximation does indeed give a good prediction for the position of the focus, particularly in region A. Figure 21 shows the corresponding time of focus of the quadratic approximation, which is not as accurate as the prediction of the position. This can be explained in terms of the 'curvature' $\mathrm{d}^2U/\mathrm{d}x^2$ of the current, as this is related to the strength of the focusing. For all x away from $x = 0$, the 'curvature' in the quadratic case is greater than in the sinusoidal case, so the focusing effect of the internal wave is stronger and the focus is earlier.

The close relation between the focusing effects of the quadratic and sinusoidal currents in this region of the velocity-ratio parameter space leads us to presume that the focusing in the sinusoidal case is non-generic. That is, to leading order, consideration of figure 18 for the quadratic current suggests that the focusing by a sinusoidal current is near perfect and the position and time of the focus is related only to the 'curvature' $\mathrm{d}^2U/\mathrm{d}x^2$ at $x = 0$. Instead of the generic $x \sim t^{3/2}$, we expect

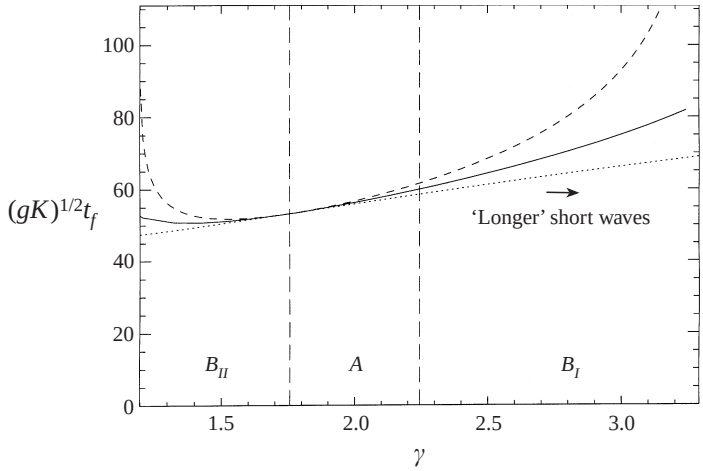

FIGURE 21. Ray-theory prediction of time of focus against γ for $\theta = 0.122$: numerical results (———), quadratic approximation ($\cdots$) and point of reflection of the $x_0 = 0$ ray (- - - -).

$x \sim t^{3/4}$. This can be shown by doing a local analysis in the region close to the focus which assumes that the rays are approximately straight lines and considers the ray envelope. Further, when considering the exact quadratic solution given by (17), we see that this is a periodic solution. This periodic focusing is also observed for the sinusoidal current for these initial conditions, i.e. if longer times are considered then the rays are seen to focus, defocus and then refocus. See, for example, figure 22, where we have taken $(\theta, \gamma) = (0.245, 2.416)$ which corresponds to the 'stronger current' case discussed previously. This refocusing is expected in relation to the periodic nature of the constant frequency solution shown in figure 2, where the rays sweep back and forth between two caustics. Similarly, for our case of initially constant wavenumber, the foci are equidistant from $x = 0$ and are periodic. Note, however, that for the fully nonlinear solution with the strength of current shown in figure 22, breaking occurs before the second focus is reached.

6.2. *Comparison with the position of reflection of the $x_0 = 0$ ray*

As was noted earlier, the quadratic focus occurs on the point of reflection of the ray originating from $x_0 = 0$. We note that this coincides with the sinusoidal focus when $\gamma = 2(1 - \theta)$. This can be shown by consideration of (7). For c to be real, $1 + 4\omega U(x)/g \geqslant 0$ which reduces to the condition

$$\cos(Kx) \geqslant \frac{1}{\theta}\left(1 - \frac{\gamma^2}{4}\left(\frac{1}{\gamma + \theta\cos(Kx_0) - 1}\right)\right). \tag{24}$$

This gives the bound for the region within which a ray starting from x_0 can propagate. If $\gamma = 2(1 - \theta)$ and $x_0 = 0$, then (24) reduces to $\cos(Kx) \geqslant 1$, i.e. $x = 0$ for all time. A ray starting from $x_0 < 0$ propagates initially to the left whereas a ray starting from $x_0 > 0$ initially propagates to the right. Two rays, one each side of the $x_0 = 0$ ray, will reflect and meet each other on $x_0 = 0$.

Figure 20 compares the position of the focus calculated numerically using the sinusoidal current with the point of reflection of the $x_0 = 0$ ray in the frame of reference moving with the internal wave; similarly, figure 21 compares the time at which focusing occurs. As with the quadratic approximation, this prediction for the position of the focus works well, especially away from the outer parts of regions B_I

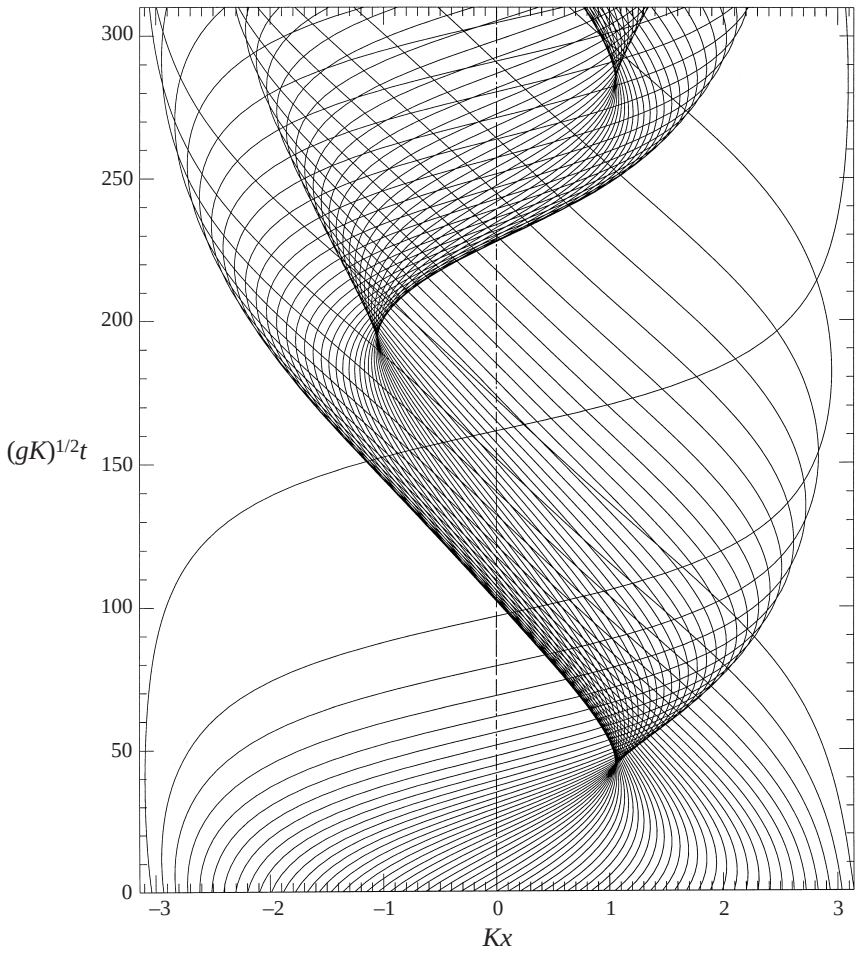

FIGURE 22. Ray paths for a stronger current showing refocusing. The frame of reference is moving with the internal wave. $(\theta, \gamma) = (0.245, 2.416)$.

and B_{II}. However, the prediction for the time shown in figure 21 works well only close to $\gamma = 2(1-\theta)$. The rays focus earlier than the point of reflection of the $x_0 = 0$ ray in regions B_I and B_{II} away from $\gamma = 2(1-\theta)$.

6.3. *General focusing behaviour in the* (θ, γ) *velocity-ratio parameter space*

In order to see the general trends of position and time of focus, we present ray-theory solutions in the (θ, γ) velocity-ratio parameter space. Figure 23 shows a contour plot of the position of focus for $0 < \theta < 0.4$ and $1 + \theta < \gamma < 4$. Contours are shown at unit intervals of Kx. The corresponding plot showing the time of focus is given in figure 24, where contours are plotted at intervals of 10 non-dimensional time units. Figure 23 is not fully covered since an upper bound on the computation time limited the time of focus.

Figure 23 shows that, as discussed above, when $\gamma = 2(1-\theta)$ the focus occurs on $x = 0$. For $\gamma > 2(1-\theta)$ the focus occurs in $x > 0$ and for $\gamma < 2(1-\theta)$ the focus occurs in $x < 0$. However, we must remember that this contour plot gives results in the frame of reference moving with the phase speed of the internal wave. Examples of the variation

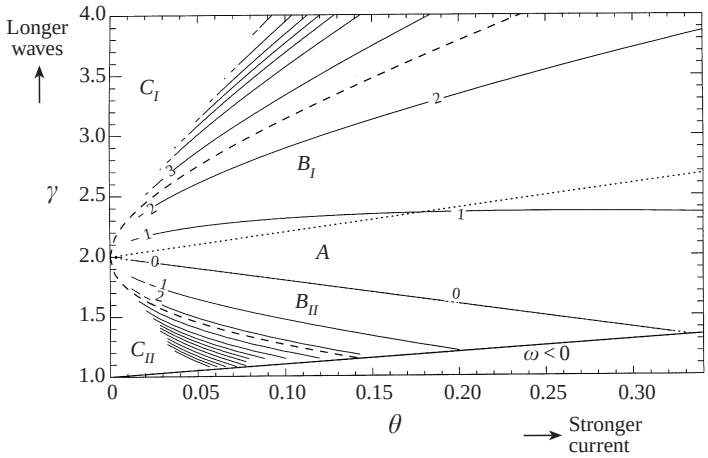

FIGURE 23. Contour plot in the (θ, γ) parameter space, showing position of focus, relative to the internal wave, for initially uniform surface waves. Contours are at unit intervals of Kx.

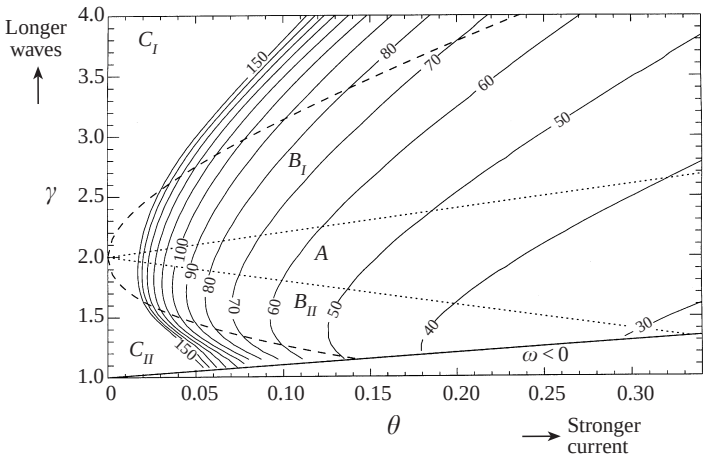

FIGURE 24. Contour plot in the (θ, γ) parameter space, showing time of focus for initially uniform waves. Contours are at intervals of 10 non-dimensional time units.

of the position of the focus in the fixed frame of reference are given in figures 25 and 26. Although these figures are for θ and γ fixed respectively, figure 23 indicates that the graphs will look qualitatively the same for a fixed, $O(1)$, value of θ, and for any value of γ. Figure 25 shows that, as γ varies, the position of the focus occurs a minimum distance from the generation of the surface waves close to $\gamma = 2(1 - \theta)$. This figure also shows that the focus can occur across a large range of phase of the internal wave, depending on the wavelength of the surface gravity waves. Figure 26 shows that the position of the focus remains almost constant relative to the maximum surface current position and, as one might expect, stronger currents focus waves more rapidly.

In regions C_I and C_{II}, the focus occurs later and the rays stay together in a 'narrow' region for some time before dispersing (see, for example, figure 8, where (θ, γ) is in region C_I). It is possible to make a rough approximation for the speed of the wave

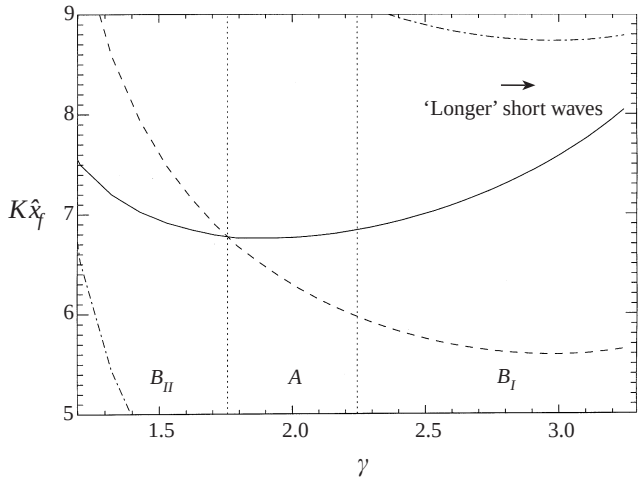

FIGURE 25. Ray-theory prediction of position of focus against γ for $\theta = 0.122$: frame of reference is fixed. Maximum surface current (— — —), minimum surface current (— · — · — · —).

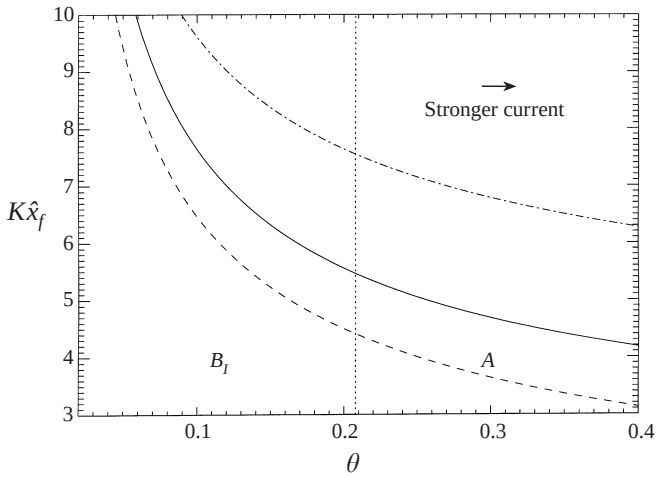

FIGURE 26. Ray-theory prediction of position of focus against θ for $\gamma = 2.416$: frame of reference is fixed. Maximum surface current (— — —), minimum surface current (— · — · — · —).

packet by making the assumption $\gamma \gg \theta$. This gives

$$\frac{\mathrm{d}x}{\mathrm{d}t} = V\left(\frac{\gamma - 2}{2} + O(\theta)\right). \tag{25}$$

This constant speed is given by the dotted line in figure 8. The (numerically calculated) position of the focus of these rays has been used as a fixed point on this line. Note that this figure is shown in a fixed frame of reference.

7. Conclusions

We have attempted to model the interaction of an underlying internal wave with a large number of short waves on the sea surface in order to explain pictures such as that shown in figure 1 and radar returns from other surfaces over inter-

nal waves, such as occur in ship wakes. This has been done by taking a simple model giving a sinusoidal form for the surface current which is steady if considered in a frame of reference moving with the phase speed of the internal wave, and has a uniform near-surface layer. The short surface waves are assumed to be of initially constant wavenumber and their interaction with the surface current has been considered as time progresses. Although this is a special initial condition, the character of the solutions has a generic form with the occurrence of wave focusing. In addition, waves generated by a single gust of wind do have almost uniform wavenumber.

By making the problem dimensionless, it is reduced to the consideration of just three parameters: two velocity-ratio parameters θ and γ defined by

$$\theta = \frac{U_c}{V} \quad \text{and} \quad \gamma = \frac{c_1}{V} = \left(\frac{g}{k}\right)^{1/2} \frac{1}{V}, \tag{26}$$

where g is acceleration due to gravity, k is the initial wavenumber of the short waves, V is the phase speed of the internal wave and U_c is the maximum magnitude of the surface current. The third parameter is ak, the initial steepness of the short surface waves. The problem can then be considered in terms of seeing how the length of the short waves, strength of current and initial steepness of the short waves affect the resultant sea surface.

After setting up this simplified model, we have found solutions using two different methods: fully nonlinear computations and linear ray theory. The former method shows nonlinear effects such as breaking, and self-focusing, but calculations are computationally very intensive and a maximum of only 20–30 surface waves can be considered per wavelength of the internal wave. In the physical situations we are concerned with, we would like to consider up to several hundred short waves per wavelength of the internal wave. However, it is possible to vary the depth of pycnocline or thermocline, and densities in the two layers and consider fewer short waves corresponding to the same situation, i.e. the same values of θ and γ. The ray theory is much quicker computationally but results are not valid in regions where rays touch, that is on caustics and at the focus. Also, only two of the three governing parameters need be considered using the linear ray theory as the amplitude, a, is just a simple multiplier in the linear theory.

The ray theory gives a prediction of the time and place of focusing of the rays. We have shown that if the sinusoidal surface current is locally approximated by a linearly varying current then the rays do not focus, and if a quadratic current is considered then a perfect focus is formed. The place and time of first focus for rays from initially uniform waves has been plotted in the (θ, γ)-plane. However, regions of high concentration of rays, for example close to the focus, correspond to steepening of waves which may cause breaking when nonlinear effects are included. The steepness of the initial waves has been varied in the fully nonlinear calculations for the different cases of 'longer' short waves and stronger current.

For many practical cases, e.g. for initial steepness $ak = 0.1$, waves steepen to breaking well before a focus occurs. However, the presence of strong focusing implies that very weak wave motion can be amplified to give waves of significant steepness, e.g. see figure 7 where waves of initial steepness $ak = 0.01$ are amplified to breaking.

It is interesting to see how the surface pattern relates to the position and wavelength of the underlying internal wave. For initially quite short waves corresponding to smaller values of γ, the focusing and hence breaking of the waves occurs in the

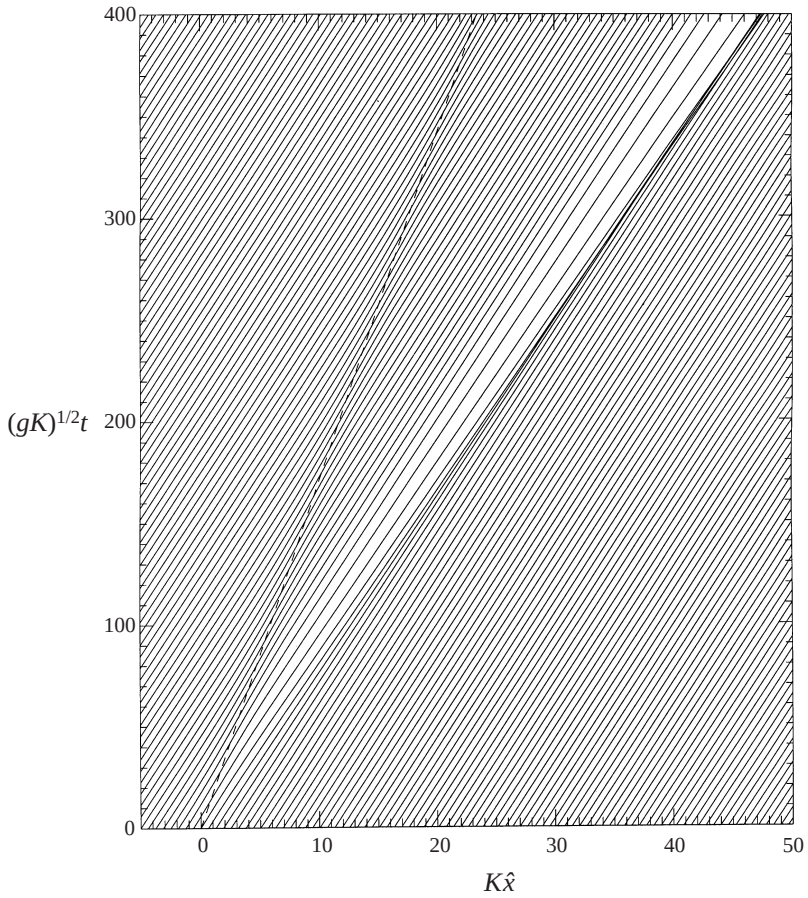

FIGURE 27. Ray paths for a solitary internal wave. The frame of reference is fixed. $(\theta, \gamma) = (0.122, 3.821)$.

region between the crest and trough of the internal wave. However, if initially 'longer' surface waves (larger γ) or 'very short' surface waves (γ close to 1) are considered, the wave packet of steeper waves which forms at the focus propagates across the internal wave almost regardless of the position of the crests and troughs of the internal wave. However, the speed of this propagating wave packet compared with that of the underlying internal wave can be well predicted by the linear ray theory. Also, it is found that 'longer' surface waves break later whereas a stronger current causes breaking to occur earlier.

As a further illustration we briefly consider a solitary internal wave which generates a surface current of the form

$$U(\hat{x}, t) = \pm \frac{U_c}{\cosh^2((K\hat{x} - \Omega t)/\sqrt{2})}, \tag{27}$$

which represents either a crest or trough of the sinusoidal surface current dependent on water depth and stratification. As expected, when the strength of current and initial length of the short waves causes focusing in $Kx \in [-\pi/2, \pi/2]$, the difference between the focusing caused by the sinusoidal current and that caused by the solitary wave current are small. For 'longer' surface waves, when in the sinusoidal case we

had a wave packet which propagated almost independently of the underlying wave, the situation is shown in figure 27 for a negative surface current. We see that the focusing of the wave packet happens in much the same way as in figure 6, except that there is a 'shadow' of longer waves propagating behind the wave group for large times. It is also interesting to note the behaviour of the constant-frequency waves coming in from $K\hat{x} = -\infty$ as they pass over the minimum in the surface current: the waves shorten and then lengthen again.

To sum up, this study has neglected surface tension and viscous effects, so it is mainly relevant to waves with lengths of 20 cm or more. It confirms the generally known effect that waves are generally steeper above internal wave crests. The relatively strong focusing and its repetition for sufficiently short surface waves adds to our understanding of the wave processes that occur. The results for somewhat longer waves give cause for concern if too simplistic an interpretation of wave patterns is made. Figures 6 and 8 show enhanced wave activity which is periodic in space. However, although it is caused by a periodic internal wave the periodic surface wave pattern has a markedly different phase velocity.

Ray theory results are complemented by accurate fully nonlinear computations. For very small initial wave steepnesses these computations also give accurate linear solutions. Although the total number of surface waves that can be computed is restricted, a sufficiently large number of waves per internal wavelength appears to have been achieved. Only a few of the many results that can be obtained from the computations are presented. In particular, the general pattern of wave behaviour predicted by ray theory is confirmed, and the occurrence of wave breaking is found.

We acknowledge the financial support of the EPSRC and the DERA; also, Mark Jervis who helped to improve the accuracy of the nonlinear code.

REFERENCES

Alpers, W. 1985 Theory of radar imaging of internal waves. *Nature* **314**, 245–247.

Berry, M. V. 1981 Singularities in waves. In *Les Houches lecture series XXXV* (ed. R. Balian, M. Kléman & J.-P. Poirer), pp. 453–543, North-Holland.

Bretherton, F. P. & Garrett, C. J. R. 1968 Wavetrains in inhomogeneous moving media. *Proc. R. Soc. Lond.* A **302**, 529–554.

Crapper, G. D. 1984 *Introduction to Water Waves*. Ellis Horwood Ltd.

Dold, J. W. 1992 An efficient surface-integral algorithm applied to unsteady gravity waves. *J. Comput. Phys.* **103**, 90–115.

Dold, J. W. & Peregrine, D. H. 1986 An efficient boundary-integral method for steep unsteady water waves. *In Numerical Methods for Fluid Dynamics* II (ed. K. W. Morton & M. J. Baines), pp. 671–679, Oxford University Press.

Gargett, A. E. & Hughes, B. A. 1972 On the interaction of surface and internal waves. *J. Fluid Mech.* **52**, 179–191.

Gasparovic, R. F., Apel, J. R. & Kasischke, E. S. An overview of the SAR internal wave signature experiment. *J. Geophys. Res.* **93**, 12304–12316.

Hogan, G. G., Chapman, R. D., Watson, G. & Thompson, D. R. 1996 Observations of ship-generated internal waves in SAR images from Loch-Linnhe, Scotland, and comparison with theory and in-situ internal wave measurements. *IEEE Trans. Geoscience and Remote Sensing* **34**, 532–542.

Jonsson, I. G. 1990 Wave–current interactions. In *The Sea*. Ocean Engineering Science vol. 9, Part A (ed. B. le Mihauti & D. M. Haine), pp. 65–120, Wiley-Interscience.

Longuet-Higgins, M. S. & Stewart, R. W. 1964 Radiation stress in water waves, a physical discussion with application. *Deep-Sea Res.* **11**, 529–562.

Osborne, A. R. & Burch, T. L. 1980 Internal solitons in the Andaman sea *Science* **208**, 451–460.

Peregrine, D. H. 1976 Interaction of water waves and currents. *Adv. Appl. Mech.* **16**, 9–117.

Peregrine, D. H. 1991 Breaking water waves. In *Nonlinear Topics in Ocean Physics* (ed. A. R. Osborne), pp. 499–526, North Holland.

Peregrine, D. H. & Smith, R. 1979 Nonlinear effects upon waves near caustics. *Phil. Trans.* R. Soc. Lond. A **292**, 341–370.

Rizk, M. H. & Ko, D. R. S. 1978 Interaction between small-scale surface waves and large-scale internal waves. *Phys. Fluids* **21**, 1900–1907.

Shuchman, R. A., Lyzenga, D. R. & Lake, B. M. 1988 Comparison of joint Canada–U.S. ocean wave investigation project Synthetic Aperture Radar data with internal wave observations and modeling results. *J. Geophys. Res.* **93**, 12283–12291.

Tanaka, M. 1983 The stability of steep gravity waves. *J. Phys. Soc. Japan* **52**, 3047–3055.

Trulsen, K. & Mei, C. C. 1993 Double reflection of capillary/gravity waves by a non-uniform current: a boundary-layer theory. *J. Fluid Mech.* **251**, 239–271.

Watson, G. 1994 Internal waves in a stratified shear-flow – the Strait of Gibraltar. *J. Phys. Oceanogr.* **24**, 509–517.

Watson, G., Chapman, R. D. & Apel, J. R. 1992 Measurements of the internal wave wake of a ship in a highly stratified sea loch. *J. Geophys. Res.* **97**, 9689–9703.

Watson, G. & Robinson, I. S. 1990 A study of internal wave-propagation in the Strait of Gibraltar using shore-based marine radar images. *J. Phys. Oceanogr.* **20**, 374–395.

White, B. S. & Fornberg, B. 1998 On the chance of freak waves at sea. *J. Fluid Mech.* **355**, 113–138.